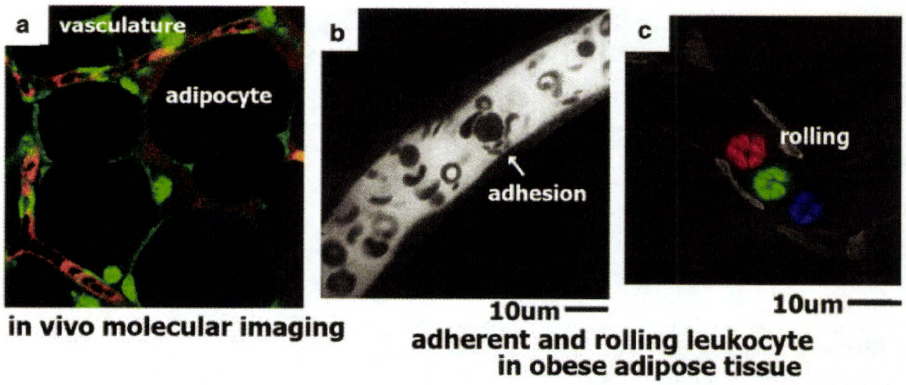

Fig. 3 Inflammatory cellular dynamics in the microcirculation of obese adipose tissue. One-shot (**a**, **b**) and sequential (**c**) images obtained by intravital fluorescence microscopy in adipose tissue from wild-type (**a**) and obese ob/ob (**b**, **c**) mice. Blood cells were negatively visualized after the injection of fluorescein isothiocyanate (FITC)-dextran [**a** (*red* and *light*), **b**]. Erythrocyte, leukocyte, and platelet cell dynamics were visualized at high spatio-temporal resolutions. The nuclei of circulating leukocytes, adipocytes, and endothelial cells were stained by acridine orange dye [**a** (*green* and *white*), **c**]. Note the firmly adherent/rolling leukocytes with small platelet aggregations on the vascular wall in the post-capillary venules of obese adipose tissue indicating inflammatory cellular dynamics (**b**, **c**). *Scale bars* 10 μm (color figure online)

function within lean and obese adipose tissue in vivo with high spatio-temporal resolution (Fig. 3). We found increased leukocyte–platelet–endothelial cell interactions in the microcirculation of obese visceral adipose tissue in ob/ob and high-fat diet-induced obese mice that were indicative of activation of the leukocyte adhesion cascade, a hallmark of inflammation. Local platelet activation in obese adipose tissue was indicated by increased P-selectin expression and the formation of monocyte–platelet conjugates. The upregulated expression of adhesion molecules on macrophages and endothelial cells suggests that their interactions contribute to local activation of inflammatory processes in obese visceral adipose tissue. Interestingly, enhanced leukocyte–endothelial interactions were not observed in subcutaneous fat in the same mice. The administration of anti-ICAM1 antibody normalized the cell dynamics seen in visceral fat, indicating that the adhesion molecules can be a new therapeutic target for obese and diabetic conditions.

CD8+ effector T cells contribute to macrophage recruitment and adipose tissue inflammation in obesity

Recently, we found that large numbers of CD8+ effector T cells infiltrated epididymal adipose tissue in obese mice, whereas the numbers of CD4+ helper and regulatory T cells decreased. The infiltration of CD8+ T cells preceded the accumulation of macrophages during diet-induced-obesity. The immunological and genetic depletion of CD8+ T cells reduced inflammatory (M1) macrophage infiltration and adipose tissue inflammation and ameliorated systemic insulin resistance. The transfer of CD8+ T cells to CD8-deficient mice enhanced inflammation in obese adipose tissue, demonstrating the importance for CD8+ T cells in obese conditions. Coculture and other in vitro experiments revealed major interactions between CD8+ T cells, macrophages, and hypertrophied adipocytes. Several in vitro studies have shown that obese adipose tissue directly activates CD8+ T cells, which subsequently promotes the recruitment and activation of macrophages, thereby initiating and maintaining the inflammatory cascades in obese adipose tissue. Infiltration of CD8+ T cells is, therefore, essential for the initiation and development of adipose inflammation [6].

Platelet kinetics in thrombus formation and inflammatory status

It is well-known that platelets play an important role in inflammatory diseases, such as atherosclerosis. However, the molecular and cellular mechanisms of platelet kinetics in vivo are unknown because experimental methodology to analyze the kinetics of individual platelets in living animals is not well established. We have already established an in vivo visualization system which enabled us to analyze thrombus formation at the individual platelet level (Fig. 4) [7]. Using this system, we are able to analyze platelet kinetics in vessels of various sizes, including large-sized arteries, veins, and small capillaries. In un-stimulated conditions, we observed that a single platelet moved in a "stop-and-go" manner along the vessel wall and interacted with endothelial cells. By inducing the production of ROS by laser injury, we can trigger thrombus formation in vessels of all sizes, including small capillaries and the carotid arteries, and observe the kinetics of individual platelets. This has enabled us to evaluate not only thrombus formation but also platelet functions at the individual

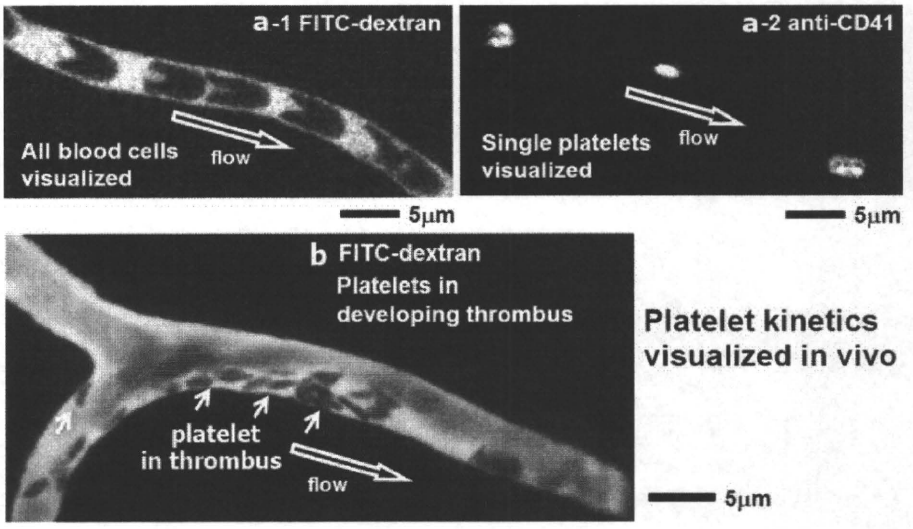

Fig. 4 Platelet kinetics in vivo in stable conditions and during thrombus development. Multi-cellular dynamics (erythrocyte, leukocyte, and platelet) in the microcirculation can be visualized with high time and spatial resolutions by injecting FITC-dextran (**a-1**). Platelets can be specifically visualized using fluorescent anti-CD41 antibody (**a-2**). **b** The developing thrombus and kinetics of the individual platelets can be visualized by in vivo imaging following laser-induced injury of the endothelium. *Scale bars* 5 μm

platelet level. Following laser injury, we observed that the platelets started to adhere to the vascular wall and to aggregate. The thrombus caused a decreased blood flow, and the vessel was subsequently completely occluded. Therefore, our imaging technique has very broad applications, such as in the evaluation of anti-platelet drugs in vivo, stem cell-derived platelet function in vivo, and the effect of genetic mutations on platelet functions.

Discussion

Cellular reactions in inflammation are particularly dynamic and involve multiple cell types. Consequently, analysis of the multi-cellular dynamic processes involved in inflammation by in vivo imaging using intact tissues in living animals represents a powerful tool. Our results demonstrate the advantages and potential of our imaging technique to analyze multi-cellular interactions in inflammation in vivo. Using our new imaging technique to analyze the complex cellular interactions within obese adipose tissue, we were able to show that visceral adipose tissue obesity is an inflammatory disease. Our technique can be used to evaluate potential therapeutic interventions against inflammation in obesity. Clearly, further studies are needed to identify what initiates the cascade of inflammatory responses in obesity. To address this important question, it will be necessary to combine in vivo visualization technologies with genetic and pharmacological interventions.

References

1. Hotamisligil GS. Inflammation and metabolic disorders. Nature. 2006;444:860–7.
2. Weisberg SP, McCann D, Desai M, Rosenbaum M, Leibel RL, Ferrante AW Jr. Obesity is associated with macrophage accumulation in adipose tissue. J Clin Invest. 2003;112:1796–808.
3. Nishimura S, Manabe I, Nagasaki M, Seo K, Yamashita H, Hosoya Y, Ohsugi M, Tobe K, Kadowaki T, Nagai R, et al. In vivo imaging in mice reveals local cell dynamics and inflammation in obese adipose tissue. J Clin Invest. 2008;118:710–21.
4. Xu H, Barnes GT, Yang Q, Tan G, Yang D, Chou CJ, Sole J, Nichols A, Ross JS, Tartaglia LA, et al. Chronic inflammation in fat plays a crucial role in the development of obesity-related insulin resistance. J Clin Invest. 2003;112:1821–30.
5. Nishimura S, Manabe I, Nagasaki M, Hosoya Y, Yamashita H, Fujita H, Ohsugi M, Tobe K, Kadowaki T, Nagai R, et al. Adipogenesis in obesity requires close interplay between differentiating adipocytes, stromal cells, and blood vessels. Diabetes. 2007;56:1517–26.
6. Nishimura S, Manabe I, Nagasaki M, Eto K, Yamashita H, Ohsugi M, Otsu M, Hara K, Ueki K, Sugiura S, et al. CD8+ effector T cells contribute to macrophage recruitment and adipose tissue inflammation in obesity. Nat Med. 2009;15:914–20.
7. Nishimura S, Takizawa H, Takayama N, Oda A, Nishikii H, Morita Y, Kakinuma S, Yamazaki S, Okamura S, Tamura N, et al. Lnk regulates integrin alphaIIbbeta3 outside-in signaling in mouse platelets, leading to stabilization of thrombus development in vivo. J Clin Invest. 2010;120:179–90.

THE JOURNAL OF BIOLOGICAL CHEMISTRY VOL. 285, NO. 32, pp. 24494–24507, August 6, 2010

Essential *in Vivo* Roles of the C-type Lectin Receptor CLEC-2

EMBRYONIC/NEONATAL LETHALITY OF CLEC-2-DEFICIENT MICE BY BLOOD/LYMPHATIC MISCONNECTIONS AND IMPAIRED THROMBUS FORMATION OF CLEC-2-DEFICIENT PLATELETS[*][S][◆]

Received for publication, April 5, 2010, and in revised form, May 11, 2010 Published, JBC Papers in Press, June 4, 2010, DOI 10.1074/jbc.M110.130575

Katsue Suzuki-Inoue,[a1,2] Osamu Inoue,[a1,3] Guo Ding,[b] Satoshi Nishimura,[c,d,e] Kazuya Hokamura,[f] Koji Eto,[g] Hirokazu Kashiwagi,[h] Yoshiaki Tomiyama,[i] Yutaka Yatomi,[j] Kazuo Umemura,[f] Yonchol Shin,[k] Masanori Hirashima,[b] and Yukio Ozaki[a]

From the [a]Department of Clinical and Laboratory Medicine, Faculty of Medicine, University of Yamanashi, 1110 Shimokato, Chuo, Yamanashi 409-3898, the [b]Division of Vascular Biology, Department of Physiology and Cell Biology, Kobe University Graduate School of Medicine, 7-5-1 Kusunoki-cho, Chuo-ku, Kobe, Hyogo 650-0017, the Departments of [c]Cardiovascular Medicine and [j]Laboratory Medicine, Graduate School of Medicine, and [d]Translational Systems Biology and Medicine Initiative, The University of Tokyo and [e]PREST, Japan Science and Technology Agency, 7-3-1 Hongo, Bunkyo-ku, Tokyo 113-8655, the [f]Department of Pharmacology, Hamamatsu University School of Medicine, 1-20-1 Handayama, Hamamatsu-shi, Sizuoka 431-3192, [g]The Stem Cell Bank, Center for Stem Cell Biology and Regenerative Medicine, The Institute of Medical Science, The University of Tokyo, 4-6-1 Shirokanedai, Minato-ku, Tokyo 108-8639, the [h]Department of Haematology and Oncology, Graduate School of Medicine C9, Osaka University, 2-2 Yamadaoka, Suita, Osaka 565-0871, the [i]Department of Blood Transfusion, Osaka University Hospital, 2-15 Yamadaoka, Suita, Osaka 565-0879, and the [k]Department of Applied Chemistry, Faculty of Engineering, Kogakuin University, 2665-1 Nakano, Hachioji, Tokyo 192-0015, Japan

CLEC-2 has been described recently as playing crucial roles in thrombosis/hemostasis, tumor metastasis, and lymphangiogenesis. The snake venom rhodocytin is known as a strong platelet activator, and we have shown that this effect is mediated by CLEC-2 (Suzuki-Inoue, K., Fuller, G. L., García, A., Eble, J. A., Pöhlmann, S., Inoue, O., Gartner, T. K., Hughan, S. C., Pearce, A. C., Laing, G. D., Theakston, R. D., Schweighoffer, E., Zitzmann, N., Morita, T., Tybulewicz, V. L., Ozaki, Y., and Watson, S. P. (2006) *Blood* 107, 542–549). Podoplanin, which is expressed on the surface of tumor cells, is an endogenous ligand for CLEC-2 and facilitates tumor metastasis by inducing platelet aggregation. Mice deficient in podoplanin, which is also expressed on the surface of lymphatic endothelial cells, show abnormal patterns of lymphatic vessel formation. In this study, we report on the generation and phenotype of CLEC-2-deficient mice. These mice are lethal at the embryonic/neonatal stages associated with disorganized and blood-filled lymphatic vessels and severe edema. Moreover, by transplantation of fetal liver cells from *Clec-2*$^{-/-}$ or *Clec-2*$^{+/+}$ embryos, we were able to demonstrate that CLEC-2 is involved in thrombus stabilization *in vitro* and *in vivo*, possibly through homophilic interactions without apparent increase in bleeding tendency. We propose that CLEC-2 could be an ideal novel target protein for an anti-platelet drug, which inhibits pathological thrombus formation but not physiological hemostasis.

The C-type lectin receptors are now established as multifunctional molecules in the field of cell adhesion, endocytosis, and pathogen recognition (1, 2). CLEC-2 (C-type lectin-like receptor-2) has been described recently as playing crucial roles in thrombosis/hemostasis, tumor metastasis, and lymphangiogenesis based on the following findings, reported mainly by us. (i) The snake venom rhodocytin is known as a strong platelet activator, and this effect has been shown to be mediated by CLEC-2 (3). (ii) Podoplanin is an endogenous ligand for CLEC-2, is expressed on the surface of tumor cells, and facilitates tumor metastasis by inducing platelet aggregation (4, 5). (iii) Mice deficient in podoplanin, which is expressed on the surface of lymphatic endothelial cells, show defects in lymphatic vessel pattern formation (6).

We have also reported that an anti-podoplanin antibody that blocks CLEC-2/podoplanin interaction inhibits tumor metastasis in an experimental lung metastasis model in mice, suggesting that CLEC-2 facilitates tumor metastasis through association with podoplanin (7). However, podoplanin is also expressed on the surface of lymphatic endothelial cells, kidney podocytes, and type I alveolar cells (8, 9). We and others found previously that podoplanin on the surface of lymphatic endothelial cells also induces platelet aggregation (4, 5). The physiological significance of this receptor/ligand interaction remains to be elucidated because lymphatic endothelial cells are not in direct contact with platelets under physiological conditions. However, it may be of great importance during organ development or under pathological conditions. It was reported previously that podoplanin-deficient mice have defects in lymphatic vessel pattern formation (6). The intracellular signaling molecules Syk (spleen tyrosine kinase) and SLP-76 (SH2 domain-containing leukocyte protein of 76 kDa) in platelets are requisites for rhodocytin-induced platelet activation mediated through CLEC-2 (3) and regulate blood and lymphatic vascular

* This work was supported in part by a grant-in-aid for scientific research from the Ministry of Education, Culture, Sports, Science, and Technology of Japan and by the Ministry of Health, Labor, and Welfare of Japan.
◆ This article was selected as a Paper of the Week.
[S] The on-line version of this article (available at http://www.jbc.org) contains supplemental Figs. 1–3, Table 1, and Videos 1 and 2.
[1] Both authors contributed equally to this work.
[2] To whom correspondence may be addressed. Tel.: 81-55-273-9884; Fax: 81-55-273-6713; E-mail: katsuei@yamanashi.ac.jp.
[3] To whom correspondence may be addressed. E-mail: oinoue@yamanashi.ac.jp.

separation, although these signaling molecules are not detected in the endothelium (10). This finding implies that Syk and SLP-76 work by way of blood cells. Moreover, blood/lymphatic misconnection is observed in mice deficient in endothelial cell *O*-glycan (11), the presence of which is required for podoplanin-induced platelet aggregation (4). Taken together, these findings lead to a hypothesis that podoplanin-induced platelet activation through CLEC-2 may regulate proper formation of lymphatic vessels. To address this issue, the generation of CLEC-2-deficient mice has been ardently awaited.

The powerful platelet-activating ability of CLEC-2 and its relatively specific expression in platelets and megakaryocytes imply that CLEC-2 also plays an important role in thrombosis and hemostasis. However, neither podoplanin nor rhodocytin can stimulate platelets within blood vessels. In addition, CLEC-2 ligands that play a role in thrombosis and hemostasis are not known. Therefore, the generation of CLEC-2-deficient mice has been awaited to reveal a role for CLEC-2 in thrombosis and hemostasis.

In this study, for the first time, we report on the generation and phenotype of CLEC-2-deficient mice. These mice are lethal at the embryonic/neonatal stage with blood/lymphatic misconnections. Moreover, by transplantation of fetal liver cells from *Clec-2*$^{-/-}$ or *Clec-2*$^{+/+}$ embryos, we were able to demonstrate that CLEC-2 is involved in thrombus stabilization, possibly through homophilic interactions.

EXPERIMENTAL PROCEDURES

Generation of Mice—A targeting vector to generate CLEC-2-deficient mice was designed so that part of exon 1 flanked by two *loxP* sites could be deleted by expression of Cre protein (supplemental Fig. 1*A*). ES[4] cells from C57BL/6 mice were transfected with this targeting vector, G418-resistant clones were screened by PCR, and positive clones were subjected to Southern blot analysis using a 3′-probe (supplemental Fig. 1, *A* and *B*). Nine ES clones were obtained containing the appropriately targeted disrupted allele and injected into blastocysts. Germ line transmission confirmed by PCR and Southern blotting was obtained in six independent ES cell clones (hereafter referred to as *Clec-2*$^{flox/+}$). We crossed a *Clec-2*$^{flox/+}$ mouse with a mouse that systemically expresses Cre recombinase to generate *Clec-2*$^{+/-}$ mice. The heterozygous mice were phenotypically normal and were bred to obtain homozygous mice for the allele containing the disrupted exon 1 of the *Clec-2* gene. For analysis of genotypes of *Clec-2* floxed mice, DNA was subjected to 30 cycles of amplification, with each cycle consisting of 20 s at 94 °C and 7 min at 62 °C, followed by an extension of 10 min at 74 °C on a thermal cycler using the long F2 and exon R primers, and PCR products were separated by 7.5% acrylamide gels (supplemental Fig. 1*A*). The WT allele gave a 229-bp band, whereas the floxed allele gave a 269-bp band by primers b and c (supplemental Fig. 1*C*). For analysis of genotypes of CLEC-2 null mice, DNA was subjected to 30 cycles of amplification, with each cycle consisting of 20 s at 94 °C and 7 min at 60 °C, followed by an extension of 10 min at 74 °C on a thermal cycler using the long F1 and exon R (733-bp band) primers for the WT allele and the neo R and long F2 (871-bp band) primers for the deleted allele, and PCR products were separated on 0.8% agarose gels (supplemental Fig. 1, *A* and *D*).

Lymphangiography—To visualize functional lymphatic vessels, FITC-dextran (Sigma; 2000 kDa; 8 mg/ml in PBS) was injected subcutaneously into the back of the embryonic forelimb. Lymphatic flow carrying FITC-dextran in embryos was analyzed by fluorescence microscopy (12).

Microscopy—Embryos were photographed at autopsy. For routine histology, embryos were fixed in 3.7% formalin and embedded in paraffin. Sections were stained with hematoxylin and eosin.

For immunohistochemistry, deparaffinized sections were stained with rabbit anti-mouse LYVE-1 antibody (Abcam Inc.) using Simplestain® mouse MAX-PO (rabbit; Nichirei Corp.) according to the manufacturer's instruction. For confocal microscopy, embryos (E17.5) were fixed overnight in 4% paraformaldehyde at room temperature; washed; and cryoprotected with 10% sucrose for 2 h, 20% sucrose for 2 h, and 40% sucrose overnight. The samples were then mounted in OCT (optimal cutting temperature) compound (Sakura Finetek). Cryosections (~10 μm) were incubated overnight at 4 °C with biotin-conjugated goat anti-mouse LYVE-1 antibody (R&D Systems), rat anti-mouse PECAM-1 (platelet endothelial cell adhesion molecule-1) monoclonal antibody (clone MEC13.3, BD Biosciences), and Cy3-conjugated anti-α-smooth muscle actin monoclonal antibody (clone 1A4, Sigma); developed with Cy5-labeled streptavidin (Invitrogen) and Alexa Fluor 488-conjugated donkey anti-rat IgG (Invitrogen) for 2 h at room temperature; and mounted with ProLong Gold mounting medium. The samples were analyzed by confocal laser-scanning microscopy using an Olympus FV-1000 microscope.

For immunohistochemical analysis of embryonic back skin, whole embryos were dissected between E14.5 and E17.5 and fixed overnight at 4 °C in 4% paraformaldehyde/PBS. The back skin was peeled off and further fixed overnight at 4 °C in 4% paraformaldehyde/PBS. Tissues were washed twice with PBS containing 0.2% Triton X-100 (PBS/T) at 4 °C for 30 min; blocked in PBS/T containing 1% bovine serum albumin at room temperature for 1 h; and stained overnight with American hamster anti-mouse PECAM-1 (clone 2H8, Chemicon), rabbit anti-mouse LYVE-1 (RELIATech), and rat anti-mouse TER-119 (clone TER-119, BD Biosciences) antibodies in blocking solution at 4 °C. Tissues were washed with PBS/T for 30 min three times at 4 °C and twice at room temperature, followed by overnight staining with Cy3-conjugated anti-American hamster IgG and Cy5-conjugated anti-rat IgG (Jackson ImmunoResearch Laboratories) or Alexa Fluor 488-conjugated anti-rabbit IgG (Invitrogen) in blocking solution at 4 °C. Tissues were washed with PBS/T for 30 min three times at 4 °C and twice at room temperature. The back skin was flat-mounted on slide glasses in ProLong Antifade (Invitrogen). Confocal microscopy was carried out on an Olympus FV-1000 microscope.

[4] The abbreviations used are: ES, embryonic stem; WT, wild-type; FITC, fluorescein isothiocyanate; E, embryonic day; PBS, phosphate-buffered saline; GP, glycoprotein; PE, phycoerythrin; vWF, von Willebrand factor; BSA, bovine serum albumin; TRITC, tetramethylrhodamine isothiocyanate; PPACK, D-phenylalanyl-L-prolyl-L-arginine chloromethyl ketone; FcR, Fc receptor.

Fetal Liver Transplantation—CLEC-2-deficient irradiated chimeric mice were generated as follows. Seven- to ten-week-old C57BL/6 male mice that had been kept on acidified water for one week and then on 0.017% enrofloxacin in water for 3 days were given two irradiations of 500 rads from a ^{60}Co source 3 h apart (13). The mice were then rescued by intravenous injection of 1.0×10^6 fetal liver cells from *Clec-2*$^{-/-}$ or control embryos at E13.5. The reconstituted mice were kept on 0.017% enrofloxacin in water for 3 weeks following irradiation and were used for experiments no fewer than 7 weeks following irradiation.

Platelet Preparation—Mice were killed with diethyl ether, and blood was drawn by postcava puncture and taken into 100 μl of acid/citrate/dextrose. Washed murine platelets were obtained by centrifugation as described previously using prostacyclin to prevent activation during the isolation procedure (14). Washed platelets were resuspended in modified Tyrode's buffer (14) at the indicated cell densities.

Generation of Rabbit anti-Mouse CLEC-2 Antibody—The recombinant extracellular domain of mouse CLEC-2 expressed as a dimeric rabbit immunoglobulin Fc domain fusion protein (mCLEC-2-rFc2) was generated as described previously (4). A purified polyclonal antibody specific for mouse CLEC-2 was purified by protein A-Sepharose (GE Healthcare) from the serum of a Japanese White rabbit after six immunizations with mCLEC-2-rFc2.

Western Blotting—Western blotting was performed as described previously (14). Briefly, washed murine platelets (2.0×10^8/ml) were dissolved in SDS sample buffer, separated by 4–12% SDS-PAGE, electrotransferred, and Western-blotted with anti-mouse CLEC-2 antibody.

Platelet Aggregation—Rhodocytin was purified as described previously (15). Poly(PHG), a specific GPVI agonist, was generated as described previously (16). 300 μl of washed platelets (2.0×10^8/ml) from CLEC-2 or WT chimeras was used for aggregation studies. The washed platelets were stimulated by rhodocytin (20 nM), collagen (1 μg/μl; Nycomed), U46619 (0.5 μM; Merck), ADP (5 μM; MC Medical), and PAR-4 (50 μM; Sigma), and platelet aggregation was monitored by light transmission using a Born aggregometer (PA-100, Kowa) with high speed stirring (1200 rpm) at 37 °C for 10 min.

Flow Cytometry—Whole blood drawn from mice as described above was diluted 15-fold using modified Tyrode's buffer. 25 μl of the diluted whole blood was incubated with Cy2-labeled anti-mouse CLEC-2, Cy2-labeled control rabbit IgG, PE-labeled control rat IgG (Emfret Analytics), FITC-labeled control rat IgG (Emfret Analytics), FITC-labeled anti-mouse GPVI (clone JAQ-1, Emfret Analytics), FITC-labeled anti-mouse integrin αIIb (Emfret Analytics), PE-labeled anti-mouse GPIbα (Emfret Analytics), FITC-labeled anti-mouse PECAM-1 (BD Biosciences), PE-labeled anti-mouse integrin α2 (clone HMα2, BD Biosciences), FITC-labeled control hamster IgG (Serotec), and FITC-labeled integrin β1 (Serotec) antibodies for 15 min at room temperature. For analysis of activated integrin αIIbβ3, 25 μl of diluted whole blood was stimulated with the indicated platelet agonists (20 nM rhodocytin, 20 μg/ml poly(PHG), 50 μg/ml collagen, 50 μM U46619, 40 μM ADP, and 100 μM PAR-4) for 5 min at room temperature, followed by the addition of anti-activated mouse integrin αIIbβ3 (clone Jon-A, Emfret Analytics) for 5 min at room temperature. For analysis of CD62P expression, 25 μl of washed platelets (5×10^7/ml) was used. Reactions were terminated by the addition of 400 μl of PBS, and the samples were then analyzed using a FACScan (BD Biosciences) and a CellQuest software (BD Biosciences). For detection of soluble mCLEC-2-rFc2 binding to platelets, WT or CLEC-2-deficient platelets (3×10^8/ml) were stimulated with or without 50 μM PAR-4 peptides for 5 min under non-stirring conditions. They were then incubated with 50 μg/ml recombinant mCLEC-2-rFc2 or rFc2 for 20 min. After washing with modified Tyrode's buffer, these cells were resuspended with 100 μl of PBS and stained with 2 μl of FITC-labeled anti-rabbit IgG (BD Biosciences) for 15 min. Stained cells were analyzed immediately using a FACScan and CellQuest software. Where indicated, quantification of the soluble protein binding was performed using median fluorescence intensity, and the data were expressed as the means ± S.E.

Measurement of Serotonin Release—Washed platelets (3×10^8/ml) from WT or CLEC-2 chimeras were stimulated with or without 20 nM rhodocytin, 20 μg/ml poly(PHG), or 50 μg/ml collagen for 5 min under non-stirring conditions. After spinning down the platelets, the serotonin concentration of 15 μl of the supernatant was measured using a 5-hydroxytryptamine enzyme-linked immunosorbent assay kit (DLD Diagnostika GmbH) according to the manufacturer's instructions.

Platelet Adhesion Assay—Coverslips were coated overnight at 4 °C with 50 μg/ml laminin, 50 μg/ml collagen, 200 μg/ml fibrinogen, 100 μg/ml vWF, 250 μg/ml rFc2, or 250 μg/ml mCLEC-2-rFc2. After washing twice with PBS, the coverslips were blocked with 1% fatty acid-free purified BSA in PBS for 2 h at room temperature and then rinsed with modified Tyrode's buffer. BSA-coated coverslips were prepared as a negative control. Washed murine platelets (3.0×10^7/ml) were seeded on the coverslips for 30 min at room temperature in the presence or absence of 10 μM ADP. After removal of unbound platelets, coverslips were washed with modified Tyrode's buffer, and adherent platelets were then fixed in 3% paraformaldehyde for 30 min at room temperature, permeabilized with 0.3% Triton X-100 for 5 min, and stained with TRITC-conjugated phalloidin for 2 h as described previously (17). Platelets were visualized using an inverted fluorescence microscope (IX71, Olympus) equipped with a 100×/1.30 objective lens, a monochromatic light source, and a DP-70 digital camera (Olympus). At least six images from two independent experiments were chosen at random per experiment and analyzed by two individuals, one of whom performed the analysis under blind conditions. Adherent platelets were counted (0.006 mm^2/image), and the platelet surface area was analyzed using NIH Image for Macintosh. Statistical significance was evaluated by Student's *t* test. In each case, p values <0.05 were taken as the minimum to indicate statistical significance.

Flow Adhesion Assay—Whole blood from WT or CLEC-2 chimeras was collected into a syringe and anticoagulated with 40 μM PPACK and 5 units/ml heparin. Capillary tubes (0.3 × 1.2 mm, 50 mm long) were coated overnight at 4 °C with 50 μg/ml collagen. Capillaries were washed and blocked with PBS containing 2% BSA for 2 h at room temperature. They were

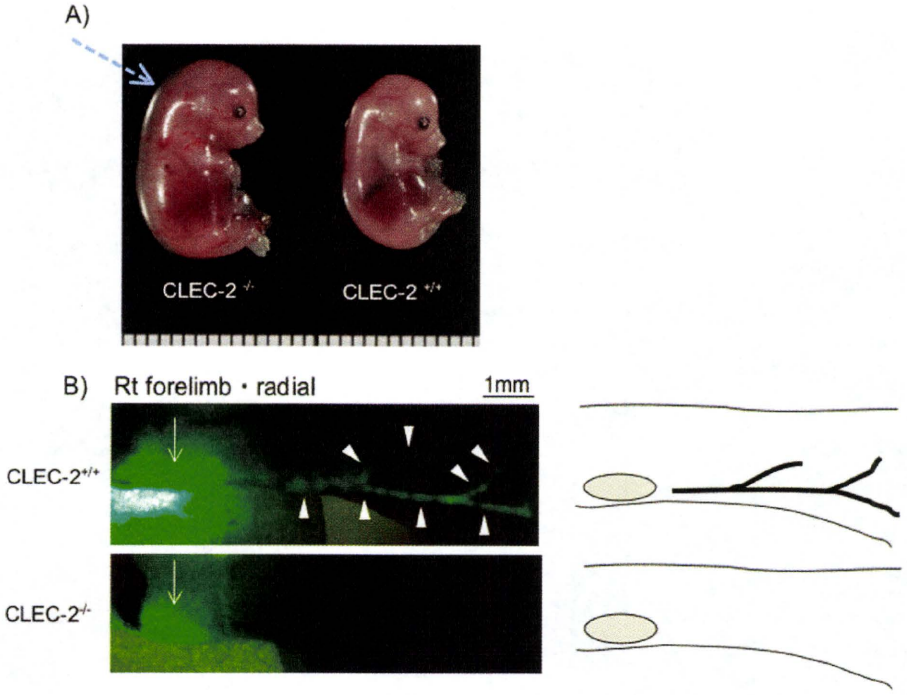

FIGURE 1. **Lymphatic function is impaired in *Clec-2*$^{-/-}$ embryos.** *A*, lateral views of E15.5 *Clec-2*$^{-/-}$ (*left*) and *Clec-2*$^{+/+}$ (*right*) embryos. Back edema in the *Clec-2*$^{-/-}$ embryo is indicated by the *arrow*. *B*, lymphangiography by injection of FITC-dextran into the forelimbs of *Clec-2*$^{+/+}$ (*upper panel*) and *Clec-2*$^{-/-}$ (*lower panel*) embryos at E17.5. Injection sites on the forelimbs are indicated by the *arrows*. The *arrowheads* indicate visualized collecting lymphatic vessels in the *Clec-2*$^{+/+}$ embryo. The *schematics* on the right illustrate the visualized collecting lymphatic vessel in *Clec-2*$^{+/+}$ mice (*upper panel*) and injection sites in *Clec-2*$^{+/+}$ (*upper panel*) and *Clec-2*$^{-/-}$ (*lower panel*) embryos (*arrow*). *Rt*, right.

then rinsed with modified Tyrode's buffer supplemented with 2 mM $CaCl_2$ and 1 unit/ml heparin and connected to a syringe filled with the anticoagulated blood that had been pretreated with 5 μM 3,3′-dihexyloxacarbocyanine iodide for 30 min. Blood was perfused into capillaries at 2000 s^{-1}, and adherent platelets were visualized using a fluorescence video microscope (IX71). Where indicated, 10 μM ADP was co-infused with the anticoagulated blood shortly before entrance into the capillary tubes. Movie data were converted into sequential photo images. For measurement of thrombus volume, capillaries with thrombus were visualized using an Olympus FV-1000 confocal microscope. The data were analyzed using FluoView software (Olympus), and thrombus volume was expressed as integrated fluorescence intensity. Platelet concentrations were counted 1 week before the experiments so that platelet counts were same between WT and CLEC-2 chimeras.

Intravital Microscopy and Thrombus Formation—To visually analyze thrombus formation in the microcirculation of the mesentery in living animals, we used *in vivo* laser injury and visualization techniques developed through modification of conventional methods (18, 19). Male mice were anesthetized by injection with urethane (1.5 g/kg), and a small incision was made so that the mesentery could be observed without being exteriorized. FITC-dextran (5 mg/kg of body weight) was injected into mice to visualize cell dynamics, whereas hematoporphyrin (1.8 mg/kg for capillary thrombi and 2.5 mg/kg for arterioles) was injected to produce reactive oxygen species upon laser irradiation. Blood cell dynamics and production of thrombi were visualized during laser excitation (488-nm wavelength, 30-milliwatt power). Sequential images were obtained for 20 s at 30 frames/s using a spinning-disk confocal microscope (CSU-X1, Yokogawa Electronics) and an electron-multiplying charged coupled device camera (iXon, Andor Technology). Platelet concentrations were counted 1 week before the experiments so that platelet counts were same between WT and CLEC-2 chimeras.

Tail Bleeding—Mice were anesthetized with 3.5% Sevoflurane and 0.5 liter/min O_2 through a face mask throughout the experiment. We laid each mouse on its stomach and arranged the tail horizontally with the tip hanging over the edge of the bench. We then cut off the tip of the tail (1 mm in length) with a sharp razor blade. The volume of blood lost during the 20-min experiment was measured. After surgical suture of the tail wound, we let the mice recover from anesthesia. Platelet concentrations were counted 1 week before the experiments so that platelet counts were same between WT and CLEC-2 chimeras.

Surface Plasmon Resonance Spectroscopy—The recombinant extracellular domain of human or mouse CLEC-2 expressed as a dimeric human or rabbit immunoglobulin Fc domain fusion protein (hCLEC-2-rFc2 and mCLEC-2-rFc2) was generated as described previously (4). A specific homophilic interaction between hCLEC-2-rFc2 or mCLEC-2-rFc2 was analyzed using a Biacore X system (Biacore AB, Uppsala, Sweden). Ligands ($\alpha v\beta 3$, $\alpha 2\beta 1$, CD62P, LIMP-II (lysosomal integral membrane protein-II), TSP-1, PEAR-1 (platelet endothelial aggregation receptor 1) (all purchased from R&D Systems), hCLEC-2-rFc2, and mCLEC-2-rFc2) were covalently coupled to a CM5 chip (Biacore AB) using an amine coupling kit (Biacore AB) according to the manufacturer's instructions (20). Regeneration of the protein-coated surfaces was achieved by running 10 μl of 10 mM HCl thorough the flow cell at 20 μl/min twice. A control surface was reacted with rFc2 and then blocked with ethanolamine. hCLEC-2-rFc2 or mCLEC-2-rFc2 in 10 mM HEPES, 0.15 M NaCl, 3 mM EDTA, and 0.005% Tween 20 (pH 7.4) (Biacore AB) at several concentrations was perfused over the control surface or an immobilized hCLEC-2-rFc2 or mCLEC-2-rFc2 surface at a flow rate of 20 μl/min at 25 °C, and the resonance changes were recorded. The response from the hCLEC-2-rFc2 or mCLEC-2-rFc2 surface was subtracted from that of the control surface. The dissociation constants (K_d) were determined using BIAevaluation software.

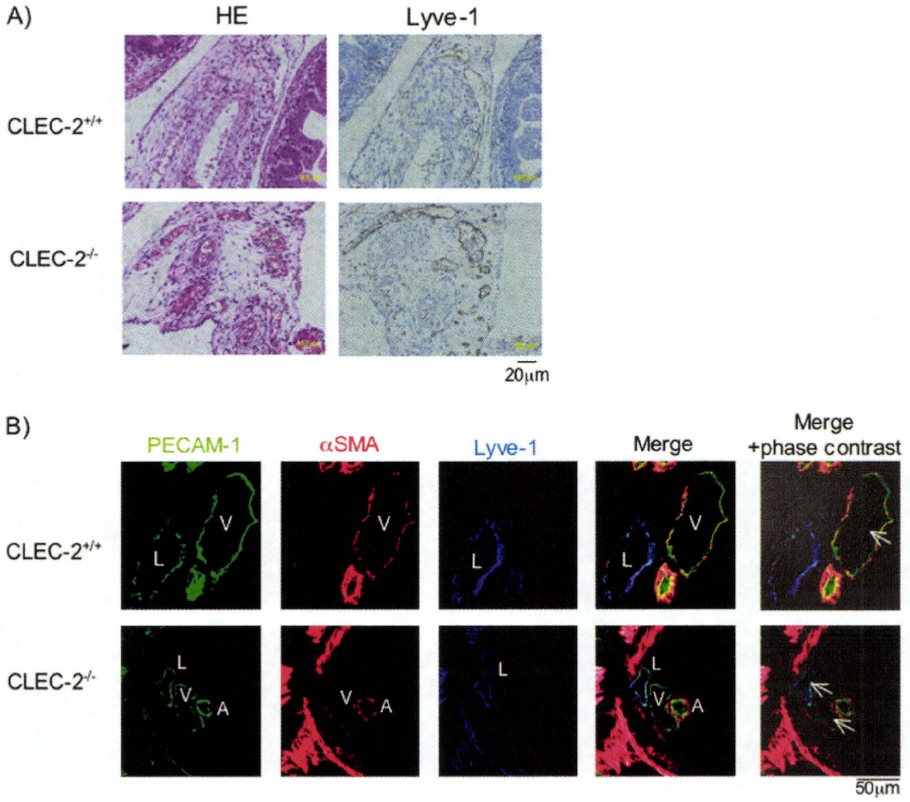

FIGURE 2. **Developing lymphatic circulation in mice lacking CLEC-2 communicates with the blood circulation.** *A*, mesenteric sections of E15.5 *Clec-2*$^{+/+}$ (*upper panels*) and *Clec-2*$^{-/-}$ (*lower panels*) embryos stained with hematoxylin and eosin (*HE*; *left panels*) and LYVE-1 (*right panels*). *B*, confocal images of intestinal cryosections of E17.5 *Clec-2*$^{+/+}$ (*upper panels*) and *Clec-2*$^{-/-}$ (*lower panels*) embryos with antibodies against PECAM-1, α-smooth muscle actin (*α-SMA*), and LYVE-1. *L*, lymphatic vessels; *V*, vein; *A*, arteries. The *arrows* indicate blood cells.

RESULTS

Generation of CLEC-2-deficient Mice—A targeting vector to generate CLEC-2-deficient mice was designed so that part of exon 1 flanked by two *loxP* sites could be deleted by expression of Cre protein (supplemental Fig. 1*A*). Nine ES clones were obtained, which contained the appropriately targeted allele, and were injected into C57BL/6 blastocysts. Southern blot analysis confirmed the presence of the targeted locus (supplemental Fig. 1, *A* and *B*). Germ line transmission was obtained from six independent ES cell clones (hereafter referred to as *Clec-2*$^{flox/+}$). We crossed a *Clec-2*$^{flox/+}$ mouse with a mouse that systemically expresses Cre recombinase to generate *Clec-2*$^{+/-}$ mice. Germ line transmission was confirmed by PCR and Southern blotting. The heterozygous mice were phenotypically normal and were bred to obtain homozygous mice for the allele containing the disrupted exon 1 of the *Clec-2* gene.

Genotype analysis of embryos from heterozygous intercrosses at E13.5 showed the expected numbers of *Clec-2*$^{-/-}$ embryos. However, the percentage of the knock-out embryos dropped to less than expected at E15.5 (supplemental Table 1). We analyzed genotypes of 326 newborn mice and found that the percentage of the knock-out mice was only 9.8% (supplemental Table 1). Moreover, most of the *Clec-2*$^{-/-}$ pups died shortly after birth, and only two *Clec-2*$^{-/-}$ mice of 326 mice survived after 8 weeks of age, suggesting that *Clec-2*$^{-/-}$ mice are lethal at the embryonic/neonatal stage. There were fewer heterozygotes than predicted by Mendelian inheritance (supplemental Table 1). We do not have any direct evidence to explain this phenomenon. It is plausible that the heterozygotes may also have some developmental abnormality related to lymphatic vessels that causes intrauterine death of some pups. This needs further investigation.

CLEC-2-deficient Mice Exhibit Disorganized Vasculature and Impaired Lymphatic Function—To investigate the cause of the embryonic or neonatal lethality of CLEC-2-deficient mice, we examined *Clec-2*$^{-/-}$ embryos. Cutaneous hemorrhagic appearance was the most striking phonotype observed in CLEC-2-lacking embryos (Fig. 1*A*), which was first noted at E12.5–E13.5. Edema was observed in the back skin in CLEC-2-deficient embryos (Fig. 1*A*, *arrow*), implying impaired lymphatic drainage. We assessed lymphatic function by infusing 2000-kDa FITC-dextran into embryonic limbs. Lymphangiography showed normal collecting lymphatic vessels immediately after dye infusion in WT mice at E17.5 (Fig. 1*B*, *upper inlet*, *arrow*), whereas dye uptake was not found even 10 min after injection (*lower inlet*), suggesting functional defects in lymphatic drainage of *Clec-2*$^{-/-}$ embryos.

Histological analysis of the mesentery of CLEC-2-deficient embryos revealed that peripheral blood cells were present within thin-walled vessels that stained for LYVE-1, a molecular marker of lymphatic endothelial cells, whereas there were no blood cells in LYVE-1-positive vessels in WT embryos (Fig. 2*A*). Triple fluorescence staining for smooth muscle actin and PECAM-1 (but not for LYVE-1) revealed that only blood vessels, but not lymphatic vessels, contained blood cells in WT embryos (Fig. 2*B*). On the other hand, lymphatic vessels as well as blood vessels contained blood cells in CLEC-2-deficient embryos (Fig. 2*B*). These findings indicate that CLEC-2-deficient mice have blood-filled lymphatic vessels.

To investigate the network formation of blood and lymphatic vessels, we performed whole-mount triple fluorescence confocal microscopy of embryonic back skin using antibodies to PECAM-1, LYVE-1, and TER-119 (a molecular marker of erythrocytes). Triple staining revealed that the dilated lymphatic vessels in CLEC-2-deficient embryos contained erythrocytes, whereas those in WT embryos did not contain blood, further confirming the blood-filled lymphatic vessels in *Clec-2*$^{-/-}$ embryos. In CLEC-2-deficient embryos, lymphatic vessels

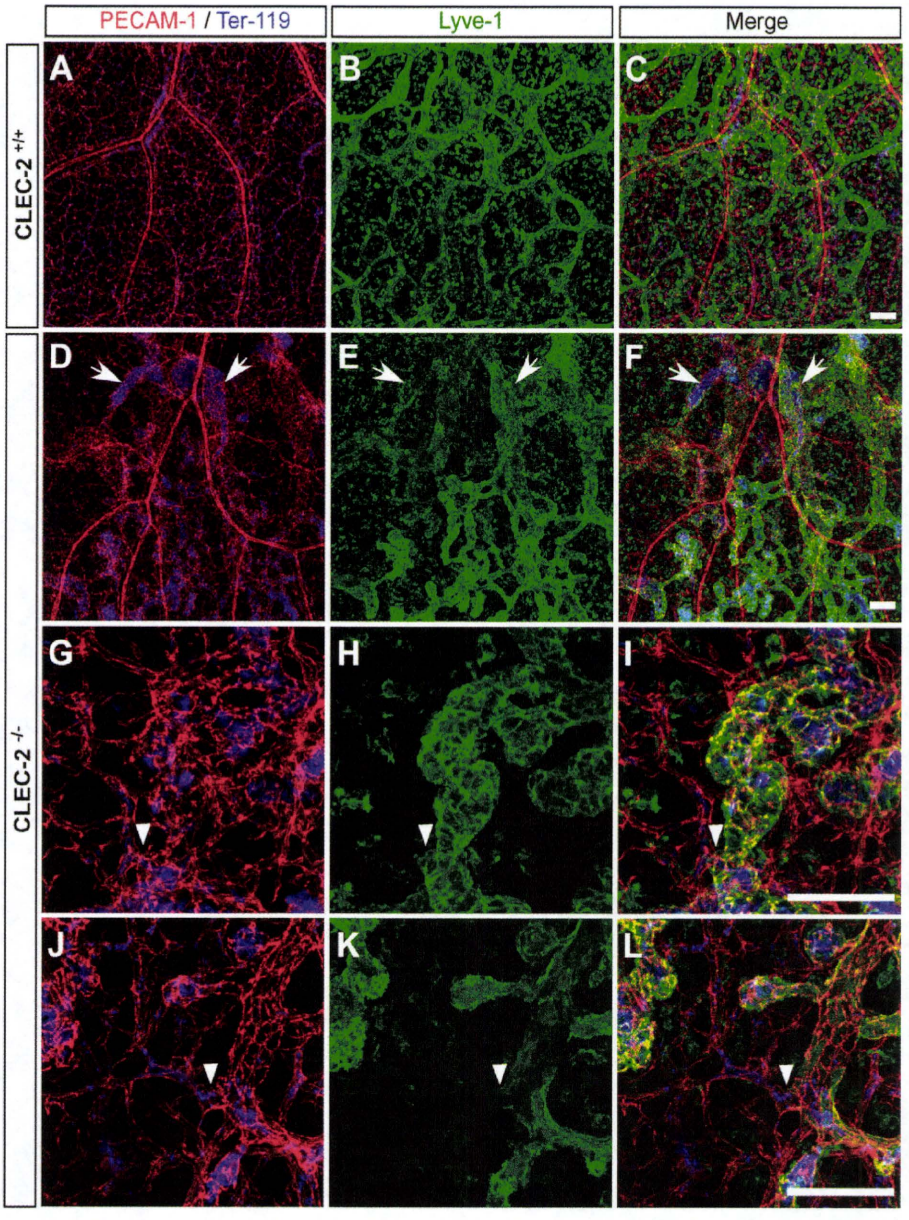

FIGURE 3. **Blood-filled disorganized lymphatic vessels and abnormal connection between blood and lymphatic vessels in *Clec-2*$^{-/-}$ embryos.** Whole-mount triple fluorescence confocal microscopy of embryonic back skin was performed with antibodies to PECAM-1 (*red*), LYVE-1 (*green*), and TER-119 (*blue*) at E14.5 (*A–I*) and E17.5 (*J–L*). *A–F*, whereas blood vessels visualized by PECAM-1 staining appear unaffected in *Clec-2*$^{-/-}$ embryos, lymphatic vessels visualized by LYVE-1 staining are disorganized and distended in *Clec-2*$^{-/-}$ embryos. Lymphatic vessels are filled with TER-119^{+} erythrocytes (*arrows*) in *Clec-2*$^{-/-}$ embryos. *G–L*, abnormal connection sites (*arrowheads*) between blood and lymphatic vessels were detected in *Clec-2*$^{-/-}$ embryos. *Scale bars* = 100 μm.

stained for LYVE-1 and PECAM-1 exhibited a dilated, tortuous, and rugged appearance, which was in contrast to the narrow, straight, and smooth appearance observed in WT embryos (Fig. 3, *A–F*). This analysis also revealed anastomotic sites of blood and lymphatic vessels in CLEC-2-deficient embryos at E14.5 (Fig. 3*I*) and at E17.5 (Fig. 3*L*).

Upon CLEC-2 simulation of platelets with rhodocytin or podoplanin, the tyrosine kinase Src phosphorylates a single YXXL motif in its cytoplasmic domain. The tyrosine kinase Syk then binds to the phosphorylated YXXL motif through its SH2 domains, which leads to Syk activation, followed by tyrosine phosphorylation of the adaptor proteins SLP-76 and LAT (linker for activation of T cells). Phospholipase Cγ2 is finally activated, which results in Ca^{2+} increase and platelet aggregation. We and others have reported previously that Src, Syk, LAT, SLP-76, and phospholipase Cγ2 are necessary for CLEC-2-mediated signal transduction (3, 21, 22). Disorganized and blood-filled lymphatic vessels observed in CLEC-2-deficient embryos were also observed in embryos deficient in Syk or SLP-76 (10) or phospholipase Cγ2 (23). These molecules are also necessary for signal transduction pathways mediated by the collagen receptor GPVI/FcR γ-chain. However, blood-filled lymphatic vessels were not observed in mice deficient in the GPVI/FcR γ-chain but only in CLEC-2-deficient mice, suggesting that platelet activation through CLEC-2, but not through the GPVI/FcR γ-chain, is important for blood/lymphatic vessel separation. We propose that CLEC-2 is essential for blood/lymphatic vessel separation, which is necessary for the survival of murine embryos.

Platelets Deficient in CLEC-2 Lack Rhodocytin-induced Platelet Activation but Show Normal Responses to Other Agonists or Extracellular Matrices—Because *Clec-2*$^{-/-}$ mice exhibited embryonic and neonatal lethality, we produced irradiated chimeric animals that had been rescued by fetal liver transplantation to investigate a role of CLEC-2 in thrombosis and hemostasis. Mice rescued with WT fetal liver are referred as WT chimeras, and those rescued with CLEC-2-deficient fetal liver are referred as CLEC-2 chimeras. Immunoblotting (Fig. 4*A*) and flow cytometry for CLEC-2 (Fig. 4*B*) confirmed successful reconstitution. CLEC-2-deficient platelets expressed major membrane proteins such as integrins αIIbβ3 and α2β1, GPIb/IX/V, and PECAM-1 at levels similar to WT platelets (supplemental Fig. 2).

In the process of physiological thrombus formation, the initial contact of platelets (tethering) to collagen exposed at sites of vessel injury is mediated predominantly by the interaction between platelet GPIb and vWF adhered to collagen, which is

essential under high shear rates. In the next step, GPVI/collagen interactions initiate cellular activation, followed by shifting of integrins to the high affinity state and the release of second-wave agonists, most importantly ADP and thromboxane A_2 (24). Released ADP and thromboxane A_2 amplify integrin activation on adherent platelets and flowing platelets, which results in platelet/platelet interaction through activated integrin αIIbβ3/fibrinogen interaction, leading to thrombus growth. Therefore, we sought to investigate the responses of CLEC-2-deficient platelets to those agonists or extracellular matrices that participate in physiological thrombus formation. CLEC-2-deficient platelets failed to aggregate in response to rhodocytin, a CLEC-2-activating snake venom, but they fully aggregated upon stimulation with other classical agonists, including ADP, U46619, collagen, and poly(PHG) (a GPVI-specific agonist peptide) (16) and thrombin receptor PAR-4-activating peptide (Fig. 4*C*). Flow cytometric analysis of integrin αIIbβ3 activation and P-selectin exposure, a marker of α-granule release, confirmed that CLEC-2 deficiency had no significant effect on platelet activation by ADP, U46619, poly(PHG), and PAR-4, whereas responses to rhodocytin were abolished (Fig. 4, *D* and *E*). Similarly, serotonin release from dense granules induced by rhodocytin, but not by poly(PHG) or collagen, was abolished in CLEC-2-deficient platelets (Fig. 4*F*). Thus, CLEC-2 deficiency results in the specific loss of the CLEC-2-mediated signal transduction pathway in platelets while leaving other pathways fully intact.

Platelets Deficient in CLEC-2 Show Normal Adhesion and Spreading on the Surface of Collagen, Fibrinogen, Laminin, and vWF—It is well known that platelets adhere and spread on the surface of various extracellular matrices such as collagen, fibrinogen, laminin, and vWF through specific receptors (collagen: integrin $\alpha2\beta1$ and GPVI; fibrinogen: integrin αIIbβ3; laminin: integrin $\alpha6$ and GPVI; and vWF: GPIb/IX/V and integrin αIIbβ3). We next investigated the possibility that CLEC-2 is a receptor for these extracellular matrices and supports platelet adhesion and spreading. As shown in Fig. 5*A*, adhesion and spreading of CLEC-2-deficient platelets on the surface of these extracellular matrices were comparable with those of WT platelets. Quantification of platelet adhesion and spreading showed that there was no statistically significance difference between CLEC-2-deficient and WT platelets (Fig. 5*B*). These findings suggest that CLEC-2 is not an activation receptor for these extracellular matrices.

CLEC-2 Is Required for Stable Thrombus Formation under Flow Conditions—Platelet activation at sites of vascular injury under flow conditions is an integrated process involving subendothelial matrices and soluble agonists, including ADP, thromboxane A_2, and thrombin, that supports adhesion and activation. To investigate a role of CLEC-2 in this process, whole blood from CLEC-2 or WT chimeras labeled with 3,3′-dihexyloxacarbocyanine iodide was flowed over collagen-coated surfaces at a high

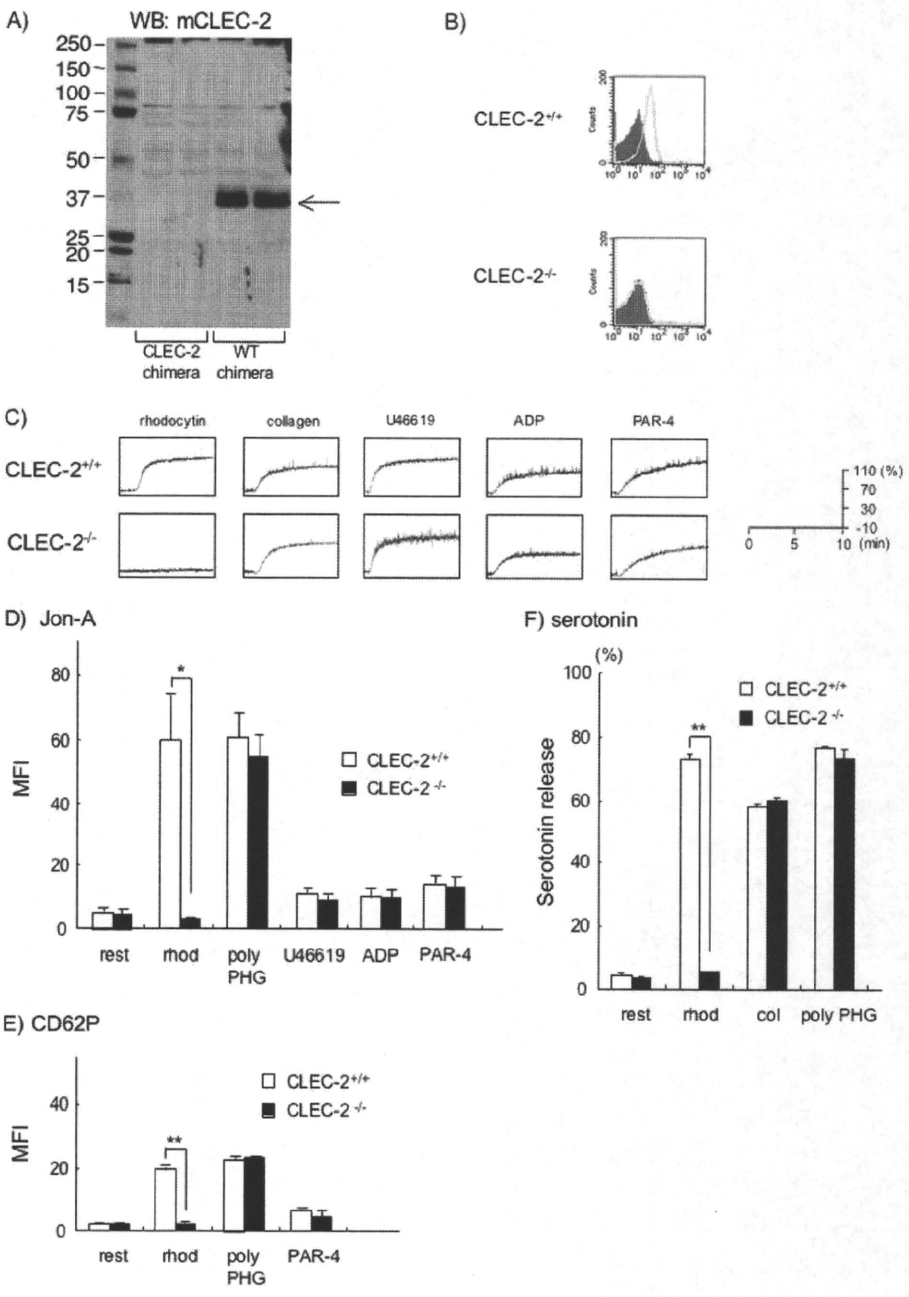

shear rate (2000 s^{-1}) for 5 min. As shown in Fig. 6 (*A–C*), WT platelets formed large thrombi on the surface of collagen by the end of a 5-min perfusion period, whereas thrombus formation of CLEC-2-deficient platelets was significantly impaired, suggesting that the CLEC-2-dependent process is essential for stable aggregate formation under flow conditions. CLEC-2-deficient platelets showed normal single-cell adhesion on the surface of collagen (Fig. 5), whereas thrombus formation on the surface of collagen under flow conditions was significantly inhibited (Fig. 6, *A–C*). Taken together, these findings suggest that CLEC-2 is required for the piling-up process of platelets that leads to stable thrombus formation, but not for initial adhesion to collagen.

To investigate whether the thrombus instability was based on impaired platelet activation, we performed flow adhesion studies with or without co-infusion of ADP, which is released from activated platelets. Co-infusion of 10 μM ADP into anticoagulated blood just before entrance into the capillary resulted in the formation of stable thrombi both in control and CLEC-2-deficient blood (supplemental Fig. 3), suggesting that CLEC-2 functions as an activation receptor in platelets that is required for stable thrombus formation.

In Vivo Thrombus Formation Is Impaired in CLEC-2 Chimeras in a Laser-induced Injury Model with Minimal Increase in Tail Bleeding—Because platelet activation/aggregation is a major cause of arterial thrombosis, we studied the effects of CLEC-2 deficiency on pathological thrombus formation. We used a direct visual technique that enabled us to evaluate *in vivo* thrombus stability with great temporal and spatial resolution and to characterize the kinetics of CLEC-2-deficient platelets in thrombus formation. This method is based on confocal microscopy, which permits high spatiotemporal resolution of individual platelets under flow conditions in mesenteric capillaries and arterioles (19, 25). With this system, laser irradiation produces reactive oxygen species, which cause injury to the endothelial layer of the vessels. In WT chimeras, after laser-induced injury to mesenteric capillaries, adherent platelets appeared to recruit platelets in the circulation to form platelet aggregates, and the resultant thrombus reduced the vessel lumen diameter and blood flow velocity. Ultimately, the lumen was completely occluded by thrombi. In contrast, CLEC-2-deficient platelets adhered to the vessel wall more loosely than WT platelets, they were frequently washed away by the blood flow, and the platelet aggregates/thrombi never occluded the capillaries (Fig. 7*A*, *panel i*, and supplemental Videos 1 and 2). As a result, the number of CLEC-2-deficient platelets that accumulated at the injured vessel was 35% less than that of WT platelets (Fig. 7*A*, *panel ii*). These findings suggest that CLEC-2 contributes to the stabilization of developing thrombi in the laser-induced injury model. We next evaluated tail bleeding of WT and CLEC-2 chimeras. Although CLEC-2 chimeras had a tendency to have more blood loss from tail bleeding than WT chimeras, it was not significant (mean blood loss ± S.E. of 13.7 ± 1.3 μl in WT chimeras and 34.7 ± 3.2 μl in CLEC-2 chimeras, $p = 0.08$) (Fig. 7*B*). Taken together, these findings suggest that CLEC-2 deficiency causes impaired thrombus growth with minimal increase in bleeding tendency.

CLEC-2 Forms Homophilic Associations—Thrombus formation under flow conditions *in vitro* and *in vivo* was impaired in CLEC-2 chimeras (Figs. 6 and 7), although CLEC-2-deficient platelets normally aggregated upon stimulation with classical agonists other than rhodocytin and showed normal adhesion and spreading on the surface of major extracellular matrices (Figs. 4 and 5). This suggests that the ligands of CLEC-2 may be present in plasma or on the surface of platelets. CLEC-2 is known to bind to podoplanin depending on glycosylation of podoplanin (4). Therefore, we first investigated the possibility of platelet membrane proteins with glycosylation, including CLEC-2 itself, as candidates for CLEC-2 ligands. To prove the interaction between the molecules directly, we utilized surface plasmon resonance (Biacore AB). Recombinant proteins of interest were perfused over the sensor tip coated with hCLEC-2-rFc2 or mCLEC-2-rFc2. Several commercially available recombinant proteins on the surface of platelet membranes, including integrins $\alpha v\beta 3$ and $\alpha 2\beta 1$, CD62P, LIMP-II, thrombospondin-1, and PEAR-1, were evaluated, but we could not observe their association with recombinant CLEC-2 (data not shown). Finally, we evaluated the CLEC-2 binding, and to our surprise, we detected homophilic interactions of hCLEC-2-rFc2 and mCLEC-2-rFc2 (Fig. 8, *A* and *B*, respectively). The sensorgrams at different analyte concentrations were obtained and normalized by subtracting background signals from the CLEC-2-Fc2 surface. The *arrows* indicate the beginning and end of perfusion of an analyte. After perfusion started, the resonance unit, which indicates the binding of analyte (flowing recombinant CLEC-2) to the ligand (coated recombinant CLEC-2), gradually increased, followed by a gradual decrease after the cessation of perfusion, suggesting that both human and mouse CLEC-2 form homophilic association. The interac-

FIGURE 4. **Responses to rhodocytin are abolished in CLEC-2-deficient platelets, but WT platelets respond normally to other agonists.** *A*, shown is a Western blot (*WB*) of washed platelets from two WT chimeras and two CLEC-2 chimeras with anti-mouse CLEC-2 antibody. The *arrow* indicates murine CLEC-2 (*mCLEC-2*). *B*, whole blood from WT and CLEC-2 chimeras was diluted 15-fold with modified Tyrode's buffer. 25 μl of the diluted whole blood was incubated with Cy2-conjugated anti-mouse CLEC-2 antibody or Cy2-conjugated control rabbit IgG for 15 min at room temperature. Reactions were terminated by the addition of 400 μl of PBS, and the samples were then analyzed using a FACScan. *C*, washed platelets from WT or CLEC-2 chimeras were used for aggregation studies. The washed platelets were stimulated by the indicated agonists, and platelet aggregation was monitored by light transmission using a Born aggregometer at 37 °C for 10 min. *D*, the activation of integrin $\alpha IIb\beta 3$ induced by the indicated agonists was investigated. Whole blood from WT or CLEC-2 chimeras was diluted 15-fold with modified Tyrode's buffer. 25 μl of diluted whole blood was stimulated with the indicated platelet agonists for 5 min at room temperature, followed by the addition of FITC-conjugated control rat IgG or FITC-conjugated anti-activated mouse integrin $\alpha IIb\beta 3$ (clone Jon-A) for 15 min at room temperature. Reactions were terminated by the addition of 400 μl of PBS, and the samples were then analyzed using a FACScan. Data are expressed as the mean of the median fluorescence intensity (*MFI*) S.E. ($n = 4–7$). *E*, CD62P expression stimulated by the indicated agonists was investigated. 25 μl of washed platelets (5×10^7/ml) was stimulated with the indicated platelet agonists for 5 min at room temperature, followed by the addition of PE-conjugated control rat IgG or PE-conjugated anti-mouse CD62P for 15 min at room temperature. Reactions were terminated by the addition of 400 μl of PBS, and the samples were then analyzed using a FACScan. Data are expressed as the mean of the median fluorescence intensity ± S.E. ($n = 4–7$). *F*, serotonin release from dense granules was investigated. Washed platelets (3×10^8/ml) were stimulated with the indicated platelet agonists for 5 min. After platelets were removed by centrifugation, the serotonin concentration of the supernatant was measured by enzyme-linked immunosorbent assay. Serotonin release is expressed as the percent serotonin concentration of the platelet lysate. Data are expressed as the mean ± S.E. ($n = 3$). *, $p < 0.05$; **, $p < 0.005$. *rhod*, rhodocytin; *col*, collagen; *rest*, resting.

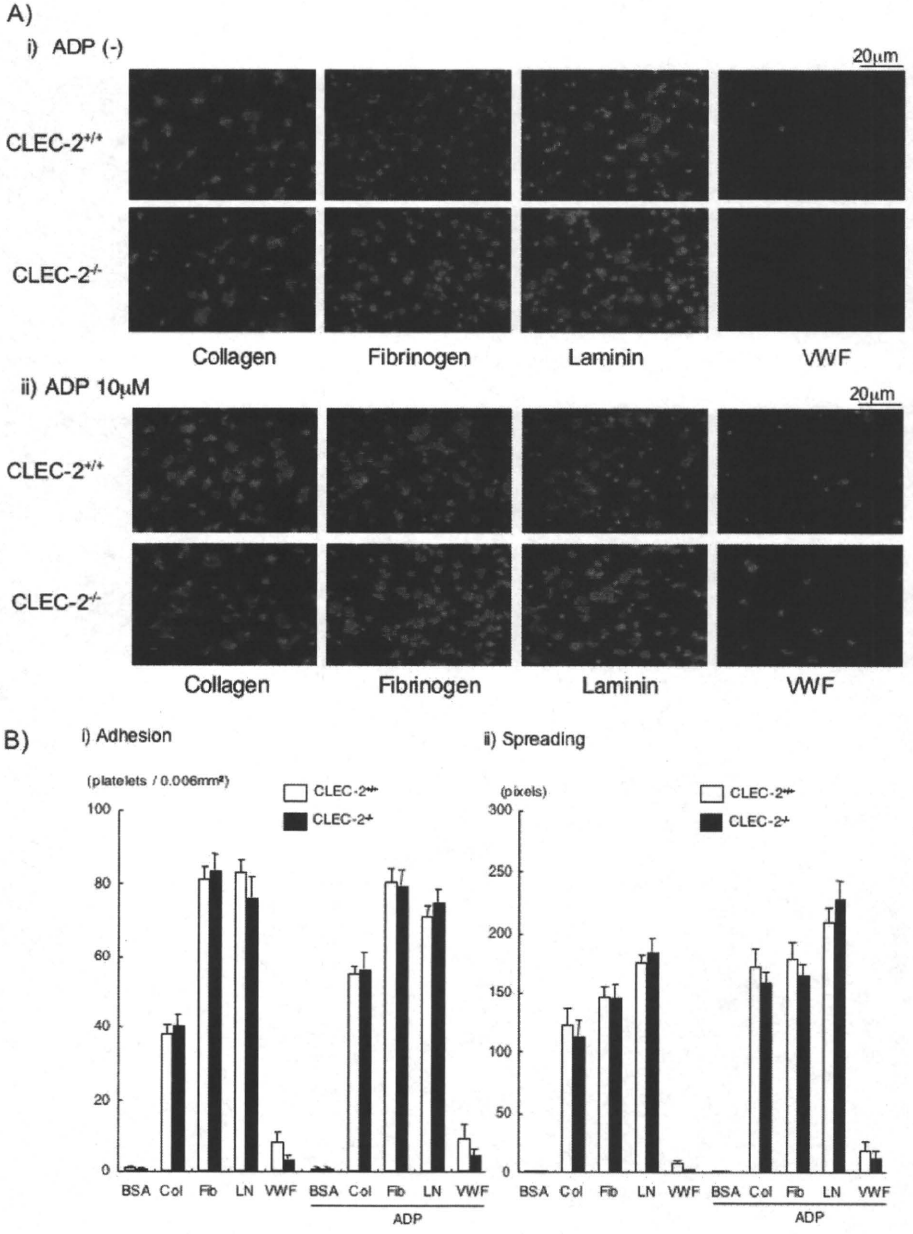

FIGURE 5. **CLEC-2-deficient platelets showed normal adhesion and spreading on the surface of collagen, fibrinogen, laminin, and vWF.** *A*, platelet spreading on the surface of major extracellular matrices was investigated. Washed platelets from WT chimeras (*Clec-2*$^{+/+}$) or CLEC-2 chimeras (*Clec-2*$^{-/-}$) were seeded on coverslips coated with laminin (*LN*), collagen (*Col*), fibrinogen (*Fib*), or vWF for 30 min at room temperature in the presence or absence of 10 μM ADP. Adherent platelets were fixed in 3% paraformaldehyde, permeabilized with 0.3% Triton X-100 for 5 min, and stained with TRITC-conjugated phalloidin. Platelets were visualized using an inverted fluorescence microscope and a digital camera. *B*, shown is the quantification of adherent platelets in the images in *A*. BSA-coated coverslips were prepared as a negative control. At least six images from two independent experiments were chosen at random per experiment and analyzed by two individuals, one of whom performed the analysis under blind conditions. Adherent platelets were counted (0.006 mm^2/image), and platelet surface area was analyzed using NIH Image.

tion between hCLEC-2-rFc2 molecules and that between mCLEC-2-rFc2 molecules were direct, with affinities of $(2.78 \pm 1.35) \times 10^{-7}$ and $(4.99 \pm 1.29) \times 10^{-7}$ M, respectively ($n = 4$) (Fig. 8*C*).

To further confirm the homophilic association of CLEC-2 under more physiological conditions, we investigated the platelet adhesion of WT or CLEC-2-deficient platelets on a surface coated with mCLEC-2-rFc2 or rFc2. To exclude the possibility that the Fc portion interacts with a stimulatory Fc receptor, FcγRIIA, we used murine platelets, which lack FcγRIIA. As shown in Fig. 9 (*A* and *B*), CLEC-2-deficient platelets adhered to collagen-coated surfaces to the same extent as WT platelets, whereas platelet adhesion to the surface of mCLEC-2-rFc2 was greatly and significantly inhibited with CLEC-2-deficient platelets ($p < 0.005$). These findings clearly suggest that CLEC-2 forms a homophilic association. Because CLEC-2-deficient platelets still adhered to mouse CLEC-2-coated surfaces and the adherent platelets showed spreading to some extent, it is likely that there is another CLEC-2 ligand on the surface of platelets.

We next investigated whether soluble recombinant CLEC-2 binds to the surface of suspended platelets by flow cytometry. As shown in Fig. 9*C*, the binding level of mCLEC-2-rFc2 to both WT and CLEC-2-deficient platelets was virtually the same as that of rFc2. However, there was a significant increase in mCLEC-2-rFc2 binding to both WT and CLEC-2-deficient platelets after platelet activation by PAR-4 peptides. However, it is important to note that the binding of mCLEC-2-rFc2 to activated WT platelets was significantly higher than that to activated CLEC-2-deficient platelets ($p < 0.05$). These findings suggest that CLEC-2 binds more avidly to CLEC-2 on the surface of activated platelets, but there appears to be another CLEC-2 ligand on the surface of activated platelets.

DISCUSSION

In this study, using CLEC-2-deficient mice for the first time, we have demonstrated that CLEC-2 is essential for blood/lymphatic vessel separation and thrombus formation *in vivo* through homophilic association. These findings imply that CLEC-2 is a potential target protein for the development of anti-platelet drugs and anti-metastatic drugs.

CLEC-2-deficient mice were lethal at the embryonic/neonatal stage with blood-filled, dilated, and tortuous lymphatic vessels that had anastomotic sites with blood vessels (blood/lym-

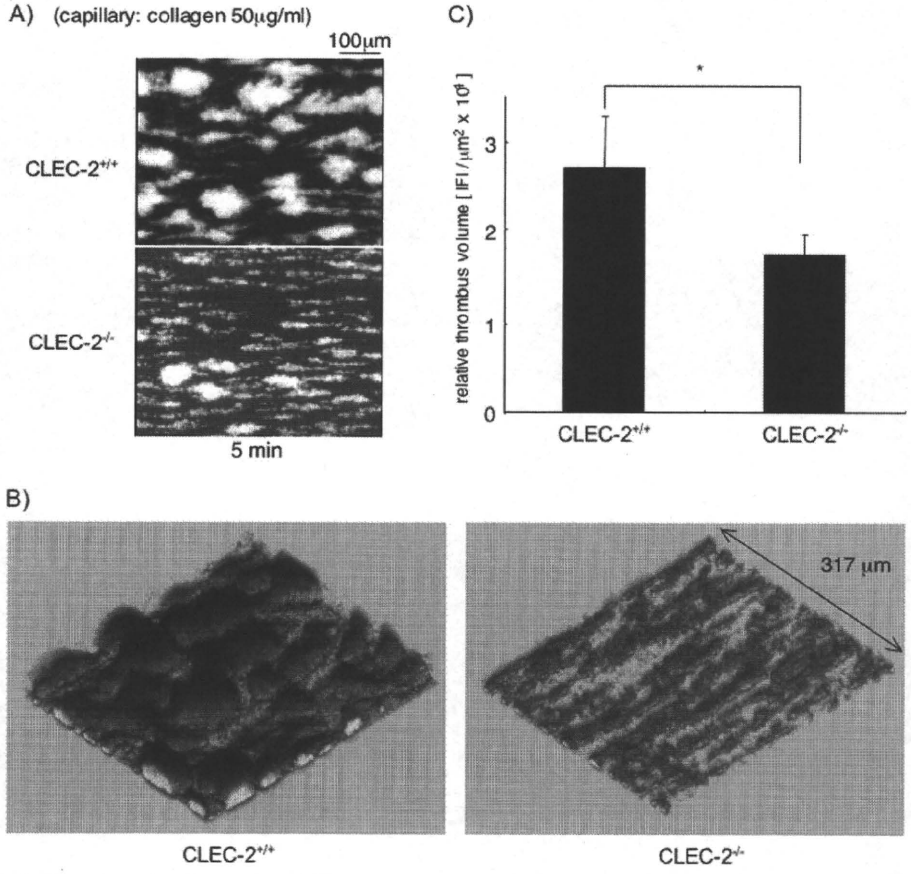

FIGURE 6. **Thrombus formation on the surface of collagen under flow conditions is impaired in CLEC-2 chimeras.** *A*, shown are video stills of thrombus formation on the surface of collagen under flow conditions. Capillary tubes were coated with 50 μg/ml collagen and blocked with PBS containing 2% BSA. Whole blood from WT chimeras (*Clec-2*$^{+/+}$) or CLEC-2 chimeras (*Clec-2*$^{-/-}$) anticoagulated with PPACK and heparin that had been pretreated with 3,3′-dihexyloxacarbocyanine iodide was perfused into capillaries at 2000 s^{-1}, and adherent platelets were visualized using a fluorescence video microscope. Movie data were converted into sequential photo images. *B*, shown are three-dimensional images of the thrombus formation. After perfusion of the blood, capillaries with thrombus were visualized using an Olympus FV-1000 confocal microscope. *C*, for measurement of thrombus volume, the images were analyzed using FluoView software, and the relative thrombus volume is expressed as integrated fluorescence intensity (*IFI*). *, $p < 0.05$ (n = at least 5 from two different mice).

phatic vessel misconnection). It is assumed that higher pressure in blood vessels drove blood components into lymphatic vessels through the anastomotic sites, resulting in dilated lymphatic vessels and retention of erythrocytes in the periphery. Progenitor cells of vascular and lymphatic endothelial cells express PECAM-1, and its expression in differentiated lymphatic endothelial cells is depressed compared with vascular endothelial cells. Although quantification has not been performed, we observed a higher level of PECAM-1 expression in the dilated lymphatic vessels in CLEC-2-deficient embryos than in WT embryos (Fig. 3, *A*, *D*, *G*, and *J*). It is plausible that blood flow from anastomosis may have led to high lymphatic pressure, which resulted in blood vessel endothelium-like change in lymphatic endothelial cells.

The mechanism by which CLEC-2 regulates blood/lymphatic vessel separation remains to be elucidated. Recently, Uhrin *et al.* (26) reported that platelet activation by podoplanin is a critical process for blood/lymphatic vessel separation. They found that platelet aggregates build up at the separation zone of podoplanin-positive lymph sacs and cardinal veins in WT embryos, but not in podoplanin-deficient embryos. Moreover, they proved that the same phenotypes are induced by anti-platelet drug, anti-podoplanin antibody, or inactivation of the *kindlin-3* gene required for platelet aggregation. We have found previously that podoplanin induces platelet aggregation through interaction with CLEC-2, and in this study, we demonstrated that CLEC-2 deficiency leads to poor blood/lymphatic vessel separation. Their findings combined with ours imply that platelet aggregates generated by CLEC-2/podoplanin interaction occlude the orifice of the lymph sacs, thereby inducing blood/lymphatic vessel separation. However, the phenotype of lymphatic vessels in podoplanin-deficient embryos is different from that in CLEC-2-deficient embryos; blood/lymphatic vessel misconnection disappears at postnatal days 10–14 in podoplanin-deficient mice, whereas the blood/lymphatic vessel misconnection is present persistently after E13.5 in CLEC-2-deficient mice. Although the majority of CLEC-2-deficient mice were lethal, we were able to obtain two adult CLEC-2-deficient mice, both of which showed the blood/lymphatic vessel misconnection phenotype (data not shown). The differences between podoplanin deficiency and CLEC-2 deficiency with regard to blood/lymphatic vessel misconnection suggest that there is a ligand (or ligands) other than podoplanin for CLEC-2 on the surface of lymphatic endothelial cells and that their interactions also play a role in blood/lymphatic vessel separation. CLEC-2 is expressed in platelets, megakaryocytes, and liver sinusoidal endothelial cells in humans and mice; however, it is also expressed in neutrophils in mice. Whether CLEC-2 in platelets, but not in neutrophils, regulates blood/lymphatic vessel separation is now under investigation using conditional knock-out mice that lack CLEC-2 only in platelets and megakaryocytes.

Although CLEC-2 plays a role in tumor metastasis, its powerful platelet-activating ability and specific expression in platelets and megakaryocytes imply that CLEC-2 also plays an important role in thrombosis and hemostasis. CLEC-2 knock-out mice should be utilized to accurately evaluate a role of CLEC-2 in thrombosis and hemostasis; however, we found that CLEC-2 knock-out mice are lethal at the embryonic/neonatal stage. We therefore generated irradiated chimeric animals that

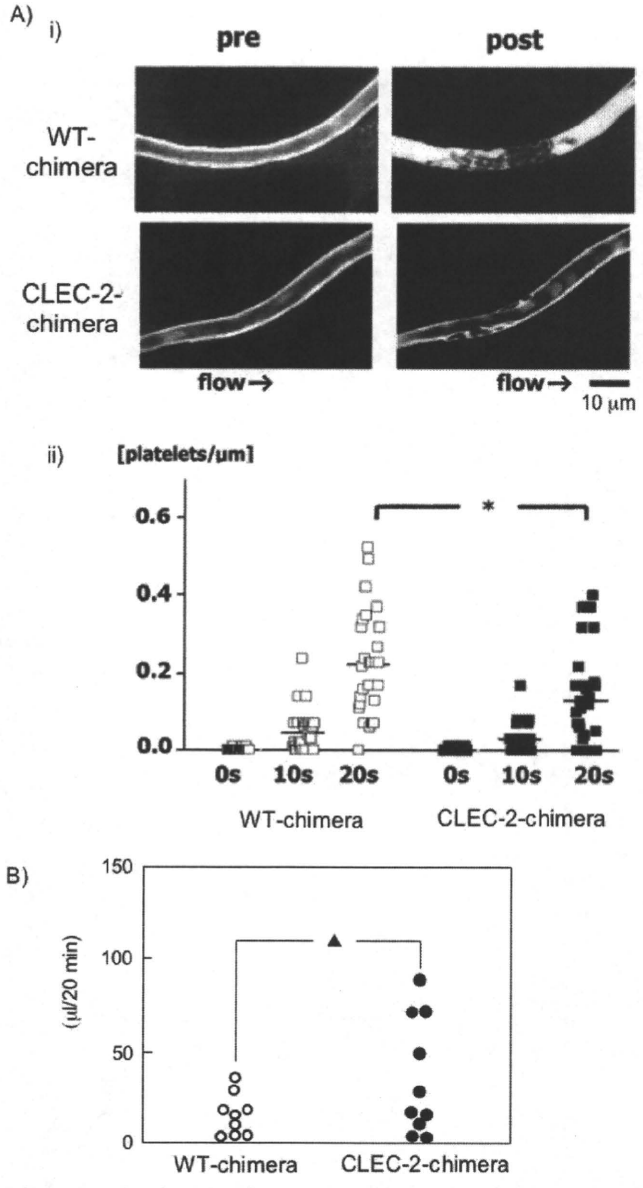

FIGURE 7. ***In vivo* thrombus formation in a laser-induced injury model is impaired in CLEC-2 chimeras without significant increase in tail bleeding.** *A*, video stills of mesenteric capillaries were obtained by intravital fluorescence microscopy before (*pre*) and 20 s after (*post*) laser-induced injury (*panel i*). The numbers of platelets in developing thrombi after laser injury to capillaries were calculated (*panel ii*). The *y axis* represents the numbers of platelets/micrometer of obtained vessel length. Results from WT and CLEC-2 chimeras 7 weeks after transplantation (17 weeks old) are shown ($n = 5$ each). *, $p < 0.05$. *B*, shown is the tail bleeding in WT and CLEC-2 chimeras. Each *symbol* represents one individual. Results from WT and CLEC-2 chimeras 8 weeks after transplantation (17 weeks old) are shown. ▲, not significant ($p = 0.08$).

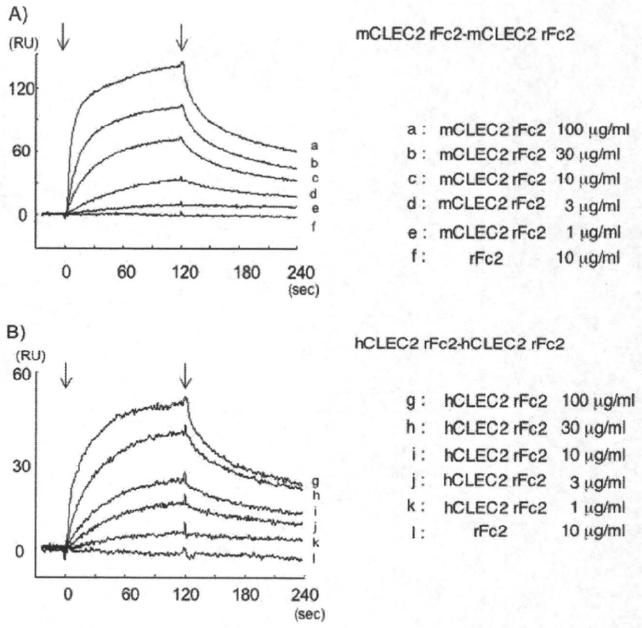

C) Dissociation constants of CLEC2

interaction	Kd ($\times 10^{-7}$)
mCLEC2 with mCLEC2	4.99 ± 1.29
hCLEC2 with hCLEC2	2.78 ± 1.35

FIGURE 8. **CLEC-2 forms a homophilic association.** Different concentrations of hCLEC-2-rFc2 (*A*) or mCLEC-2-rFc2 (*B*) were flowed over an immobilized hCLEC-2-rFc2 (*A*), mCLEC-2-rFc2 (*B*), or control surface coated with rFc2. The *arrows* indicate the beginning and end of perfusion of hCLEC-2-rFc2 and mCLEC-2-rFc2. The results are shown from one experiment that is representative of four others. *RU*, resonance units. $K_d \pm$ S.E. ($n = 4$) of homophilic association of hCLEC-2-rFc2 or mCLEC-2-rFc2 was determined as described under "Experimental Procedures" (*C*).

had been rescued by transplantation of fetal liver taken from mice lacking CLEC-2. We observed significant inhibition of thrombus formation in CLEC-2 chimeras under flow conditions *in vivo* and *in vitro*, although platelet adhesion and spreading, which are the initial steps for thrombus formation, remained intact. Moreover, the bleeding tendency was minimal with CLEC-2 chimeras (Fig. 7*B*), suggesting that low molecular weight compounds acting as CLEC-2 antagonists are ideal candidates for a novel anti-platelet drug that inhibits pathological thrombus formation, but not physiological hemostasis. CLEC-2 deficiency leads to blood/lymphatic misconnections at the developmental stage; however, this does not seem to be a problem for a CLEC-2 antagonist, as an anti-platelet drug is normally administrated to adults.

Recently, May *et al.* (27) reported that anti-CLEC-2 antibody treatment of mice leads to the loss of CLEC-2 in circulating platelets for several days. These CLEC-2-deficient platelets displayed normal adhesion under flow conditions, but subsequent aggregate formation was severely impaired *in vitro* and *in vivo*, revealing an essential function of CLEC-2 in hemostasis and thrombosis. Although this unique study by May *et al.* shed light on the physiological role of CLEC-2, there still remains room for criticism of antibody-induced removal of antigen from platelets; it may have certain undesirable effects. Extensive antigen/antibody interaction on the platelet membrane may have some effects on thrombus formation. Alternatively, antibody-induced platelet activation and subsequent release of secondary mediators may result in desensitization of platelets. In mice, CLEC-2 is also expressed on peripheral blood neutrophils, and it mediates phagocytosis of antibody-coated beads and the production of proinflammatory cytokines, including tumor necrosis factor-α upon CLEC-2 stimulation (28). It is possible that the

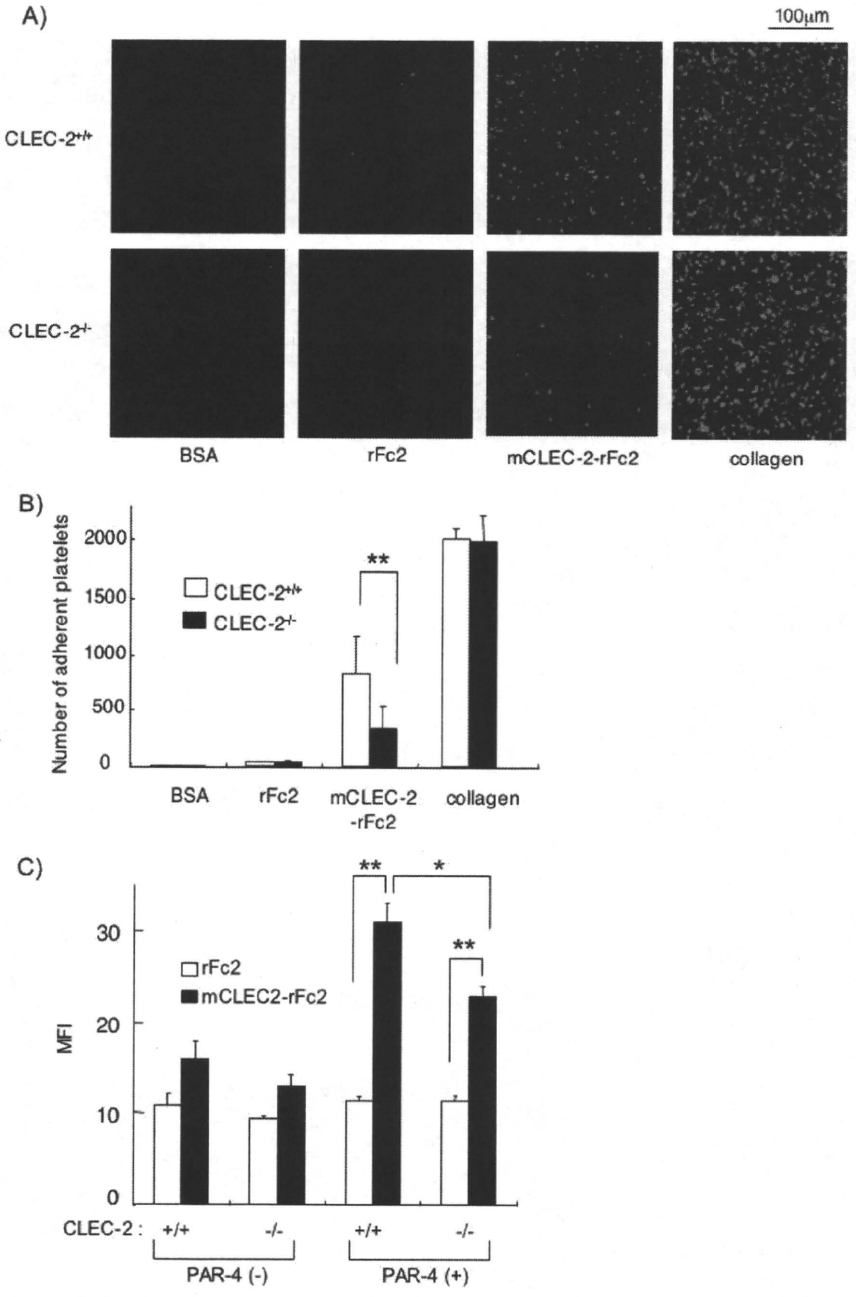

FIGURE 9. **Platelet adhesion to mCLEC-2-rFc2-coated surfaces and soluble mCLEC-2-rFc2 binding to platelets are inhibited in CLEC-2-deficient platelets.** *A*, shown is platelet adhesion on a surface coated with mCLEC-2-rFc2. Washed murine platelets from WT or CLEC-2 chimeras were seeded on coverslips coated with the indicated materials. Adherent platelets were fixed in paraformaldehyde, permeabilized with 0.3% Triton X-100, and stained with TRITC-conjugated phalloidin for 2 h. Platelets were visualized using an inverted fluorescence microscope and a digital camera. *B*, shown is the quantification of the platelet adhesion in *A*. At least six images from two independent experiments were chosen at random per experiment and analyzed by two individuals, one of whom performed the analysis under blind conditions. Adherent platelets were counted (0.006 mm^2/image). *C*, the binding of soluble mCLEC-2-rFc2 or rFc2 on the surface of WT (*Clec-2*$^{+/+}$) or CLEC-2-deficient (*Clec-2*$^{-/-}$) platelets was investigated by flow cytometry. Quantification of the soluble protein binding was performed using median fluorescence intensity (*MFI*). Data are expressed as mean ± S.E. ($n > 4$). Statistical significance was evaluated by Student's *t* test. In each case, *p* values <0.05 were taken as the minimum to indicate statistical significance. *, $p < 0.05$; **, $p < 0.005$.

anti-CLEC-2 antibody administered to mice may also work on CLEC-2 on neutrophils, thereby modifying cytokine generation and phagocytosis, which may affect thrombus formation under flow conditions or *in vivo*. In fact, it has been reported that tumor necrosis factor-α inhibits thrombus formation (29). Therefore, generation of CLEC-2-deficient mice has been awaited to solve these problems.

In our experiments, CLEC-2 chimeras showed only a mild increase in tail bleeding, which was not statistically significant compared with WT chimeras (Fig. 7*B*). In contrast to our findings, May *et al.* (27) reported that anti-CLEC-2 antibody-induced deficiency results in a marked increase in bleeding time: bleeding stopped in all of the control mice during a 20-min observation period (mean bleeding time of 6.1 ± 3.1 min), whereas bleeding continued for >20 min in 33% of the anti-CLEC-2 antibody-treated mice (mean bleeding time of 10.8 ± 6.0 min for those in which bleeding stopped). The discrepancy between gene-manipulated loss of antigen and antibody-induced loss has been reported previously; the bleeding time of GPVI/FcR γ-chain-deficient mice was not different from that of WT mice (30), whereas antibody-induced GPVI-deficient mice showed significantly increased bleeding times (158 ± 89 s in control mice *versus* 330 ± 103 s in antibody-treated mice) using the same protocol for the measurement of bleeding time. The idea of antibody-induced knock-out mice is derived from previously reported idiopathic thrombocytopenic purpura patients. Sugiyama *et al.* (31) and Moroi *et al.* (32) reported that idiopathic thrombocytopenic purpura patients contain an antibody against GPVI that stimulates platelet aggregation, leading to loss of GPVI from the platelet surfaces. These idiopathic thrombocytopenic purpura patients show a bleeding tendency, as is the case in antibody-induced GPVI- or CLEC-2-deficient mice, whereas genetically modified GPVI- or CLEC-2-deficient mice have no or less bleeding tendency. Although the precise mechanism for this discrepancy has not been elucidated, it is quite likely that antigen/antibody interaction induces some

unexpected biological responses, which may lead to overestimation of bleeding tendency due to loss of GPVI or CLEC-2.

Although it has been demonstrated that CLEC-2 is essential for thrombus formation, podoplanin, the only known internal ligand of CLEC-2 to date, is expressed in lymphatic endothelial cells or tumor cells and cannot be responsible for arterial thrombus formation. Thus, an important issue remains as to how CLEC-2 support thrombus formation under flow conditions *in vitro* and *in vivo*. From the findings of a previous work (27) and this study, it is suggested that the ligands of CLEC-2 are present in plasma or on the surface of activated platelets. We propose that CLEC-2 support thrombus formation, at least partly, through homophilic association based on the following findings. 1) Surface plasmon resonance detected homophilic association between recombinant CLEC-2 molecules. 2) Platelet adhesion onto a surface coated with recombinant CLEC-2 was significantly attenuated with CLEC-2-deficient platelets. 3) The binding of soluble recombinant CLEC-2 was significantly attenuated with CLEC-2-deficient platelets. We found that the interaction between hCLEC-2-rFc2 molecules is direct, with an affinity of 2.78×10^{-7} M, and that the affinity between mCLEC-2-rFc2 molecules is 4.99×10^{-7} M ($n = 4$). Christou *et al.* (5) reported that CLEC-2 and podoplanin interact directly, with an affinity of $(2.45 \pm 0.37) \times 10^{-5}$ M, which apparently suggests that the affinity between CLEC-2 and podoplanin is much weaker than the homophilic CLEC-2 interaction. One may argue that it is intriguing that podoplanin-expressing cells induce platelet aggregation, whereas platelets that express CLEC-2 with a high affinity homophilic interacting property do not form spontaneous aggregates. However, Christou *et al.* used monomeric recombinant CLEC-2 with a His tag and podoplanin-coated sensor chips, whereas we used dimeric recombinant CLEC-2 with Fc2, and the sensor chips were coated with this dimer form; we made dimeric CLEC-2, as it has been suggested that CLEC-2 exists as a dimer form on cell surfaces (22, 33). Because dimer forms of receptors are known to have much higher affinity for their ligands than single forms in the case of GPVI (34), this apparent discrepancy in the affinity of CLEC-2 for ligands may be due to the different experimental conditions. Alternatively, recombinant CLEC-2 fixed on the surface may assume a conformation that has higher homophilic activity than the natural CLEC-2 molecule on resting platelets, thereby giving a smaller K_d in a surface resonance study. This hypothesis may be extended to allege that CLEC-2 has two forms, one with relatively low homophilic activity in resting platelets and another with high homophilic activity in activated platelets. In support of this hypothesis, soluble CLEC-2 binding to suspended platelets was observed only after platelet activation (Fig. 9*C*). Moreover, surface expression of CLEC-2 was unaltered after stimulation (data not shown), suggesting higher homophilic binding activity of CLEC-2 in activated platelets. Additional experiments will need to address these issues.

We also assume that there are other CLEC-2 ligands on the surface of platelets than CLEC-2 itself. Although CLEC-2-deficient platelets showed reduced adhesion on the surface of recombinant CLEC-2 and reduced binding of soluble recombinant CLEC-2, it was not completely inhibited (Fig. 9). Moreover, CLEC-2-deficient platelets adhered to recombinant CLEC-2-coated surfaces showed spreading, suggesting that there is another ligand (or ligands) for CLEC-2 on the surface of platelets, the binding to which leads to platelet activation and spreading.

In conclusion, we have demonstrated, using CLEC-2-deficient mice, that CLEC-2 is essential for blood/lymphatic vessel separation and thrombus formation *in vivo* through homophilic association. We also suggest the possibility that there are other ligands for CLEC-2 that regulate lymphangiogenesis and thrombus formation. CLEC-2 is a promising target protein for the development of anti-platelet drugs that inhibit pathological thrombus formation, but not physiological hemostasis.

Acknowledgments—We are grateful to Dr. Kumiko Nakazawa, Tsutomu Yuminamochi, Chiaki Komatsu, and Hisaichiro Nakazawa for excellent technical assistance.

Note Added in Proof—During the submission of our manuscript, Bertozzi *et al.* reported that platelets regulate lymphatic vascular development through CLEC-2/SLP-76 signaling (Bertozzi, C. C., Schmaier, A. A., Mericko, P., Hess, P. R., Zou, Z., Chen, M., Chen, C. Y., Xu, B., Lu, M. M., Zhou, D., Sebzda, E., Santore, M. T., Merianos, D. J., Stadtfeld, M., Flake, A. W., Graf, T., Skoda, R., Maltzman, J. S., Koretzky, G. A., and Kahn, M. L. (2010) *Blood*, in press).

REFERENCES

1. Cambi, A., and Figdor, C. G. (2003) *Curr. Opin. Cell Biol.* **15,** 539–546
2. Marshall, A. S., and Gordon, S. (2004) *Eur. J. Immunol.* **34,** 18–24
3. Suzuki-Inoue, K., Fuller, G. L., García, A., Eble, J. A., Pöhlmann, S., Inoue, O., Gartner, T. K., Hughan, S. C., Pearce, A. C., Laing, G. D., Theakston, R. D., Schweighoffer, E., Zitzmann, N., Morita, T., Tybulewicz, V. L., Ozaki, Y., and Watson, S. P. (2006) *Blood* **107,** 542–549
4. Suzuki-Inoue, K., Kato, Y., Inoue, O., Kaneko, M. K., Mishima, K., Yatomi, Y., Yamazaki, Y., Narimatsu, H., and Ozaki, Y. (2007) *J. Biol. Chem.* **282,** 25993–26001
5. Christou, C. M., Pearce, A. C., Watson, A. A., Mistry, A. R., Pollitt, A. Y., Fenton-May, A. E., Johnson, L. A., Jackson, D. G., Watson, S. P., and O'Callaghan, C. A. (2008) *Biochem. J.* **411,** 133–140
6. Schacht, V., Ramirez, M. I., Hong, Y. K., Hirakawa, S., Feng, D., Harvey, N., Williams, M., Dvorak, A. M., Dvorak, H. F., Oliver, G., and Detmar, M. (2003) *EMBO J.* **22,** 3546–3556
7. Kato, Y., Kaneko, M. K., Kunita, A., Ito, H., Kameyama, A., Ogasawara, S., Matsuura, N., Hasegawa, Y., Suzuki-Inoue, K., Inoue, O., Ozaki, Y., and Narimatsu, H. (2008) *Cancer Sci.* **99,** 54–61
8. Schacht, V., Dadras, S. S., Johnson, L. A., Jackson, D. G., Hong, Y. K., and Detmar, M. (2005) *Am. J. Pathol.* **166,** 913–921
9. Breiteneder-Geleff, S., Matsui, K., Soleiman, A., Meraner, P., Poczewski, H., Kalt, R., Schaffner, G., and Kerjaschki, D. (1997) *Am. J. Pathol.* **151,** 1141–1152
10. Abtahian, F., Guerriero, A., Sebzda, E., Lu, M. M., Zhou, R., Mocsai, A., Myers, E. E., Huang, B., Jackson, D. G., Ferrari, V. A., Tybulewicz, V., Lowell, C. A., Lepore, J. J., Koretzky, G. A., and Kahn, M. L. (2003) *Science* **299,** 247–251
11. Fu, J., Gerhardt, H., McDaniel, J. M., Xia, B., Liu, X., Ivanciu, L., Ny, A., Hermans, K., Silasi-Mansat, R., McGee, S., Nye, E., Ju, T., Ramirez, M. I., Carmeliet, P., Cummings, R. D., Lupu, F., and Xia, L. (2008) *J. Clin. Invest.* **118,** 3725–3737
12. Hirashima, M., Sano, K., Morisada, T., Murakami, K., Rossant, J., and Suda, T. (2008) *Dev. Biol.* **316,** 149–159
13. Turner, M., Mee, P. J., Costello, P. S., Williams, O., Price, A. A., Duddy, L. P., Furlong, M. T., Geahlen, R. L., and Tybulewicz, V. L. (1995) *Nature*

378, 298–302
14. Suzuki-Inoue, K., Inoue, O., Frampton, J., and Watson, S. P. (2003) *Blood* **102,** 1367–1373
15. Shin, Y., and Morita, T. (1998) *Biochem. Biophys. Res. Commun.* **245,** 741–745
16. Inoue, O., Suzuki-Inoue, K., Shinoda, D., Umeda, Y., Uchino, M., Takasaki, S., and Ozaki, Y. (2009) *FEBS Lett.* **583,** 81–87
17. Suzuki-Inoue, K., Yatomi, Y., Asazuma, N., Kainoh, M., Tanaka, T., Satoh, K., and Ozaki, Y. (2001) *Blood* **98,** 3708–3716
18. Law, D. A., DeGuzman, F. R., Heiser, P., Ministri-Madrid, K., Killeen, N., and Phillips, D. R. (1999) *Nature* **401,** 808–811
19. Nishimura, S., Manabe, I., Nagasaki, M., Seo, K., Yamashita, H., Hosoya, Y., Ohsugi, M., Tobe, K., Kadowaki, T., Nagai, R., and Sugiura, S. (2008) *J. Clin. Invest.* **118,** 710–721
20. Inoue, O., Suzuki-Inoue, K., McCarty, O. J., Moroi, M., Ruggeri, Z. M., Kunicki, T. J., Ozaki, Y., and Watson, S. P. (2006) *Blood* **107,** 1405–1412
21. Fuller, G. L., Williams, J. A., Tomlinson, M. G., Eble, J. A., Hanna, S. L., Pöhlmann, S., Suzuki-Inoue, K., Ozaki, Y., Watson, S. P., and Pearce, A. C. (2007) *J. Biol. Chem.* **282,** 12397–12409
22. Hughes, C. E., Pollitt, A. Y., Mori, J., Eble, J. A., Tomlinson, M. G., Hartwig, J. H., O'Callaghan, C. A., Futterer, K., and Watson, S. P. (2010) *Blood* **115,** 2947–2955
23. Ichise, H., Ichise, T., Ohtani, O., and Yoshida, N. (2009) *Development* **136,** 191–195
24. Nieswandt, B., and Watson, S. P. (2003) *Blood* **102,** 449–461
25. Takizawa, H., Nishimura, S., Takayama, N., Oda, A., Nishikii, H., Morita, Y., Kakinuma, S., Yamazaki, S., Okamura, S., Tamura, N., Goto, S., Sawaguchi, A., Manabe, I., Takatsu, K., Nakauchi, H., Takaki, S., and Eto, K. (2010) *J. Clin. Invest.* **120,** 179–190
26. Uhrin, P., Zaujec, J., Breuss, J. M., Olcaydu, D., Chrenek, P., Stockinger, H., Fuertbauer, E., Moser, M., Haiko, P., Fässler, R., Alitalo, K., Binder, B. R., and Kerjaschki, D. (2010) *Blood* **115,** 3997–4005
27. May, F., Hagedorn, I., Pleines, I., Bender, M., Vögtle, T., Eble, J., Elvers, M., and Nieswandt, B. (2009) *Blood* **114,** 3464–3472
28. Kerrigan, A. M., Dennehy, K. M., Mourão-Sá, D., Faro-Trindade, I., Willment, J. A., Taylor, P. R., Eble, J. A., Reis e Sousa, C., and Brown, G. D. (2009) *J. Immunol.* **182,** 4150–4157
29. Cambien, B., Bergmeier, W., Saffaripour, S., Mitchell, H. A., and Wagner, D. D. (2003) *J. Clin. Invest.* **112,** 1589–1596
30. Mangin, P., Yap, C. L., Nonne, C., Sturgeon, S. A., Goncalves, I., Yuan, Y., Schoenwaelder, S. M., Wright, C. E., Lanza, F., and Jackson, S. P. (2006) *Blood* **107,** 4346–4353
31. Sugiyama, T., Okuma, M., Ushikubi, F., Sensaki, S., Kanaji, K., and Uchino, H. (1987) *Blood* **69,** 1712–1720
32. Moroi, M., Jung, S. M., Okuma, M., and Shinmyozu, K. (1989) *J. Clin. Invest.* **84,** 1440–1445
33. Watson, A. A., Christou, C. M., James, J. R., Fenton-May, A. E., Moncayo, G. E., Mistry, A. R., Davis, S. J., Gilbert, R. J., Chakera, A., and O'Callaghan, C. A. (2009) *Biochemistry* **48,** 10988–10996
34. Miura, Y., Takahashi, T., Jung, S. M., and Moroi, M. (2002) *J. Biol. Chem.* **277,** 46197–46204

Circulation Research
JOURNAL OF THE AMERICAN HEART ASSOCIATION

Structural Heterogeneity in the Ventricular Wall Plays a Significant Role in the Initiation of Stretch-Induced Arrhythmias in Perfused Rabbit Right Ventricular Tissues and Whole Heart Preparations

Kinya Seo, Masashi Inagaki, Satoshi Nishimura, Ichiro Hidaka, Masaru Sugimachi, Toshiaki Hisada and Seiryo Sugiura

Circ. Res. 2010;106;176-184; originally published online Nov 5, 2009;
DOI: 10.1161/CIRCRESAHA.109.203828
Circulation Research is published by the American Heart Association. 7272 Greenville Avenue, Dallas, TX 72514
 Print ISSN: 0009-7330. Online ISSN: 1524-4571

Structural Heterogeneity in the Ventricular Wall Plays a Significant Role in the Initiation of Stretch-Induced Arrhythmias in Perfused Rabbit Right Ventricular Tissues and Whole Heart Preparations

Kinya Seo, Masashi Inagaki, Satoshi Nishimura, Ichiro Hidaka, Masaru Sugimachi, Toshiaki Hisada, Seiryo Sugiura

Rationale: **Mechanical stress is known to alter the electrophysiological properties of the myocardium and may trigger fatal arrhythmias when an abnormal load is applied to the heart.**

Objective: **We tested the hypothesis that the structural heterogeneity of the ventricular wall modulates globally applied stretches to create heterogeneous strain distributions that lead to the initiation of arrhythmias.**

Methods and Results: **We applied global stretches to arterially perfused rabbit right ventricular tissue preparations. The distribution of strain (determined by marker tracking) and the transmembrane potential (measured by optical mapping) were simultaneously recorded while accounting for motion artifacts. The 3D structure of the preparations was also examined using a laser displacement meter. To examine whether such observations can be translated to the physiological condition, we performed similar measurements in whole heart preparations while applying volume pulses to the right ventricle. At the tissue level, larger stretches (≥20%) caused synchronous excitation of the entire preparation, whereas medium stretches (10% and 15%) induced focal excitation. We found a significant correlation between the local strain and the local thickness, and the probability for focal excitation was highest for medium stretches. In the whole heart preparations, we observed that such focal excitations developed into reentrant arrhythmias.**

Conclusions: **Global stretches of intermediate strength, rather than intense stretches, created heterogeneous strain (excitation) distributions in the ventricular wall, which can trigger fatal arrhythmias. (*Circ Res.* 2010;106:176-184.)**

Key Words: stretch-induced arrhythmia ■ mechanoelectric feedback ■ optical mapping

Alterations to the mechanical state of the myocardium affect its electrophysiological properties, a phenomenon termed mechanoelectric feedback (MEF).[1,2] MEF is considered to play a significant role in the genesis of cardiac rhythm disturbances in various disease states, such as myocardial infarction and heart failure, in which myocardial tissues are subjected to abnormal loading conditions.[3–5] This speculation is supported by previous observations that in myocardial infarction, ventricular ectopic excitations are initiated by acute stretches of the border zone between the infarct and the normal myocardium.[6–8] A more definite causality is suspected in the etiology of commotio cordis, where sudden death occurs owing to a nonpenetrating chest wall impact in the absence of injury to the ribs, sternum, and heart.[9,10] Using anesthetized juvenile swine, Link et al[10] found that ventricular fibrillation can be produced by a baseball strike, and examined the effects of the phase, strength and speed of the strike for the induction of arrhythmias.

To elucidate the mechanisms underlying MEF and related arrhythmias, extensive studies have been carried out using various preparations from various species, including rabbits, lambs and dogs.[11–13] Stretch-activated channels (SACs) have been regarded as the most likely candidates for the primary transducers of mechanical stress.[14–16] Although such findings at the molecular level can account for changes in the action potential duration, amplitude, effective refractory period and resting potential induced by mechanical interventions at the cellular level, we still face a huge gap between these laboratory findings and clinical arrhythmias observed at the organ level. In this context, Franz et al[17] investigated the effects of increases in ventricular volume and pressure on epicardial monophasic action potentials in both isolated cross-circulated hearts and

Original received January 17, 2008; resubmission received June 26, 2009; revised resubmission received October 23, 2009; accepted October 27, 2009.

From the Department of Human and Engineered Environmental Studies (K.S., T.H., S.S.), Graduate School of Frontier Sciences, The University of Tokyo, Chiba; Department of Cardiovascular Dynamics (K.S., M.I., I.H., M.S.), National Cardiovascular Center Research Institute, Osaka; and Department of Cardiovascular Medicine (S.N.), The University of Tokyo, Japan.

Correspondence to Masashi Inagaki, Department of Cardiovascular Dynamics, National Cardiovascular Center Research Institute, 5-7-1 Fujishirodai, Suita, Osaka 565-8565, Japan; E-mail masashii@ri.ncvc.go.jp or to Seiryo Sugiura, Department of Human and Engineered Environmental Studies, Graduate School of Frontier Sciences, The University of Tokyo 5-1-5 Kashiwanoha, Kashiwa, Chiba 277-8563, Japan; E-mail sugiura@k.u-tokyo.ac.jp

Circulation Research is available at http://circres.ahajournals.org DOI: 10.1161/CIRCRESAHA.109.203828

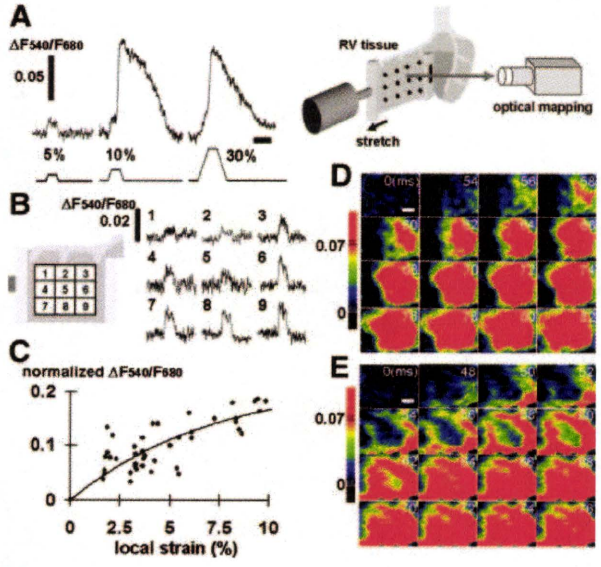

Figure 1. Alterations in the electric response in a cardiac tissue. A, Ratiometric optical signals ($\Delta F_{540}/F_{680}$) in response to 5%, 10%, and 30% stretches from left to right. Scale bar: 100 ms. B, Spatiotemporal pattern of the depolarizations (typical optical signals in each segment) in response to a 5% stretch. C, Relationship between the changes in the normalized optical signals and the local strain under the excitation threshold (n=5). The smooth curve through the data points was fitted with a nonlinear regression model. D and E, Representative action potentials and optical maps in response to 10% and 30% stretches, respectively. The stretch starts at 0 ms. Scale bar: 4 mm.

in situ canine hearts to clearly demonstrate the manifestation of MEF. However, these volume and/or pressure alterations do not allow detailed evaluation of the changes in myocardial stress or strain, which are believed to be the keys for establishing a link between the macroscopic and microscopic phenomena.

To elucidate how the cellular responses to stretches lead to arrhythmias in the heart, we focused on the morphology of tissue preparations and its role in the modulation of the electric responses. We developed an experimental set-up in which controlled uniaxial stretches were applied to crystalline perfused rabbit ventricular walls while monitoring the local strain. The use of optical transmembrane potential mapping combined with a tissue tracking technique enabled us to examine the relationship between local strain and excitation of the myocardium. By applying acute stretches of varying amplitudes, we demonstrate that global stretches applied to the ventricular wall tissue can create strain dispersion in the heterogeneous structure of the ventricular wall and that mechanical insults of intermediate, rather than intense, strength induce focal excitation, thus potentially triggering fatal arrhythmias. Finally, using whole heart preparations, we confirm that only medium stretches of the myocardium can evoke spiral wave formation.

Methods

Japanese white rabbits weighing 2.4 to 2.9 kg were used. The distribution of strain and the transmembrane potential were simultaneously recorded while applying an acute stretch to right ventricle (RV) tissue preparations. The 3D structure of the preparations was also examined. Similar measurements were conducted in whole heart preparations while applying acute volume pulses to the RV.

An expanded Methods section is available in the Online Data Supplement at http://circres.ahajournals.org.

Non-standard Abbreviations and Acronyms

MEF	mechanoelectric feedback
SAC	stretch-activated channel
RV	right ventricle

Results

Effect of the Stretch Amplitude on Excitation of the Tissue

To elucidate the relationship between the electric response and the stretch level, we measured the optical transmembrane potential signals of stretched tissues. Figure 1 shows representative transmembrane potential signals in response to stretches of varying amplitudes. When a uniaxial stretch with a small amplitude (5%) was applied, the myocardial tissue was depolarized but an action potential did not develop (Figure 1A, left). The distribution of these depolarizations was heterogeneous and the amplitudes of these depolarizations had a positive dependence on the local strains (n=5) (Figure 1B and 1C). However, above a certain level of amplitude (≥10%), we observed focal excitation (development of an action potential in less than 4 segments of 9 blocks) (Figure 1A, middle; Figure 1D). A larger stretch (30%) only induced multiple occurrences of excitation in the tissue (Figure 1E). Figure 2A shows the relationship between the probability of tissue excitation (development of an action potential in at least one locus within the tissue) and the amplitude of the stretch applied (global strain). We found a fairly abrupt transition in the tissue responses to a uniaxial stretch (n=7). Specifically, excitation was rare when the amplitude was small (5%), but its rate increased with stretches in the medium range (10% and 15%) to reach 100% (sure observation) in response to large stretches (20%, 25% and 30%).

The use of a trapezoidal command with constant rates of rise and fall necessarily made the entire duration of the stretch longer for larger stretches, which may thus have led to modulation of the responses of the myocardium through different mechanisms. To exclude these possibilities, we applied stretches of varying amplitudes while keeping the entire duration constant at 50 ms. We found similar responses, thereby indicating that the amplitude rather than the duration is the major determinant of stretch-induced activation of the myocardium (Online Figure V, A). We also confirmed that stretches applied during the action potentials could modulate their shapes, and sometimes found stretch-activated depolarizations followed by premature ventricular contractions (Online Figure V, B).

Relationship Between Stretch-Induced Excitation and Epicardial Local Strain

We also evaluated the relevance between stretch-activated excitation and epicardial local strain (n=7). To compare the

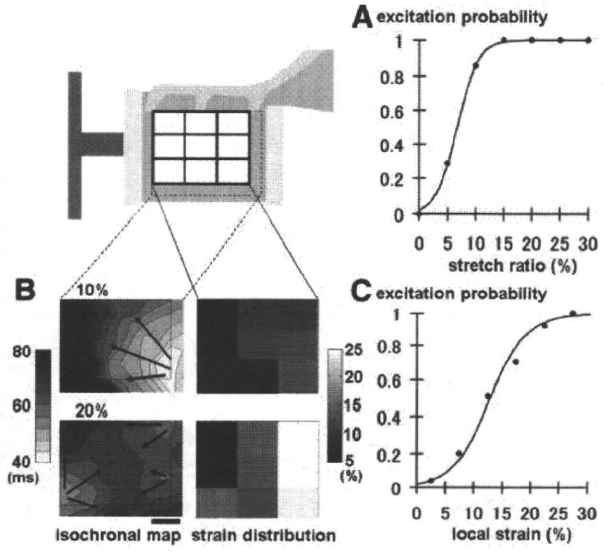

Figure 2. Electric responses and strain distributions. A, Probability that an action potential develops in at least 1 region of the whole tissue as a function of global stretch (n=7). The smooth curve through the data points was fit with a logistic regression model. B, Representative isochronal maps of a transmembrane potential showing the point of initial depolarization (left) and distributions of local strain (right). Top and bottom show 10% and 20% stretch, respectively. Scale bar: 4 mm. C, Relationship between the probability of stretch-induced excitation in the local area and the strain in the corresponding area (n=7). The smooth curve through the data points was fit with a logistic regression model.

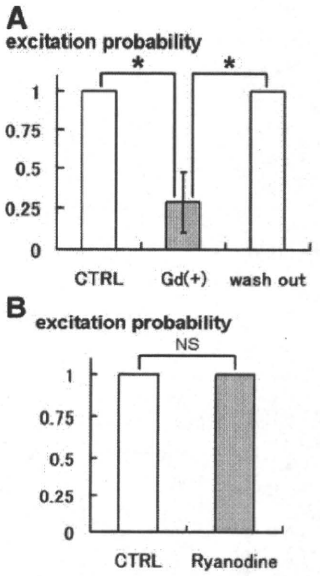

Figure 3. Modulation of stretch-induced excitation by drugs. A, Effect of Gd^{3+} on the probability of stretch-induced excitation after a 15% stretch (n=7). *$P<0.05$. CTRL indicates control condition. B, Effect of ryanodine on the probability of stretch-induced excitation after a 15% stretch (n=3).

strain distribution with the isochronal electric responses, the whole tissue area was divided into 9 blocks and the average strain value in each block was shown in grayscale. The local strain maps at each level of stretch with the corresponding isochronal maps are shown in Figure 2B (right). Initial excitation tended to take place at the locus of high strain (top: right lower block with 14% strain; bottom: left lower block with 14% strain; right upper 2 blocks with 23% and 24% strains). The excitation probability was clearly found to be more prominent for higher strains (Figure 2C), when the probability of local excitation was plotted as a function of the corresponding local strain (n=7).

Involvement of SACs in Stretch-Induced Excitations

To examine the involvement of SACs in the genesis of stretch-induced excitation, we repeated the experiments with a 15% stretch in the presence of 10 μmol/L Gd^{3+}, a blocker of nonspecific SACs. Gd^{3+} inhibited the stretch-induced excitation by 71.4±18.4% compared with the control condition and its effect was reversed by washout of Gd^{3+} (Figure 3A; n=7; $P<0.01$, Gd(+) versus control condition and washout). We also administered ryanodine to examine whether stretch-induced Ca^{2+} release from the sarcoplasmic reticulum and the triggered activity are involved in the activation process. When we applied 15% stretches, action potentials developed similarly in both ryanodine-treated and untreated (control condition) tissues (Figure 3B; n=3).

Strain Distribution and Tissue Structure

Because we applied uniaxial stretches to the ventricular tissue, the strain distribution on the epicardial surface was most probably created by heterogeneity within the tissue structure. To clarify the relationships between the strain distribution and the tissue structure, we measured the thickness distribution in each preparation using a laser displacement meter (Figure 4A; n=7). We divided the tissue into 9 blocks and calculated the average thickness in each block to facilitate comparisons with the strain data. Figure 4B shows a comparison between the thickness and local strain distributions after a 10% stretch from a single experiment. We found that the strain was high in regions where the tissue thickness was thin. For further comparisons between the tissue structure and the strain, we calculated the normalized thickness value of each block (mean thickness value of each block relative to the mean thickness value of all the blocks). Figure 4C summarizes the relationships between the local strain and the local thickness under different levels of stretch. Local strain was negatively correlated with the local thickness, which supported our hypothesis (10% stretch: n=7, $r=-0.52$, $P<0.0001$; 20% stretch: n=7, $r=-0.53$, $P<0.0001$).

Heterogeneous Excitation in Accordance With the Tissue Thickness and Stretch Level

We then plotted the relationship between the local wall thickness and the probability of stretch-induced local excitation for various levels of stretches (Figure 5A; n=7; closed circles, 5% stretch; closed triangles, 15% stretch; open circles, 30% stretch). When the applied stretch was small (5%), there was hardly any excitation (low probabilities over the entire range of thickness) because the local strain was below the threshold. As the amplitude of the stretch increased, the probability of excitation started to rise from the